LATE MIDDLE TO LATE MIOCENE PALEOCEANOGRAPHY AT ROCKALL PLATEAU SITE 982

By

OLIVER JOHN MCLELLAN

A thesis submitted to the

School of Graduate Studies

Rutgers, The State University of New Jersey

In partial fulfillment of the requirements

For the degree of

Master of Science

Graduate Program in Earth and Planetary Sciences

Written under the direction of

Kenneth G. Miller

And approved by

New Brunswick, New Jersey

January 2020

ABSTRACT OF THE THESIS

Late Middle to Late Miocene Paleoceanography at Rockall Plateau Site 982

by OLIVER JOHN MCLELLAN

Thesis Director:

Kenneth G. Miller

The Middle and Late Miocene were associated with a global cooling trend, with the development of a permanent East Antarctic Ice Sheet during the Middle Miocene Climate Transition (MMCT; 14.8-12.8 Ma), increased influence of Northern Component Water at ~12 Ma, and a more rapid rate of cooling during Late Miocene Cooling (LMC; ~8-6 Ma). Possible causes of these variable sea surface temperatures (SSTs) throughout the Miocene are changes in the amount of carbon dioxide in the atmosphere (pCO_2) and shifts in the magnitude of meridional heat transport via Atlantic Meridional Ocean Circulation (AMOC). Biomarker temperature proxies ($U^{k'}_{37}$ and TEX_{86}) from the North Atlantic have previously been used to track Miocene SST variability. I employ an analysis of foraminiferal stable isotope ratios from the late Middle Miocene to Early Pliocene at Ocean Drilling Program (ODP) Site 982 Hole B (57.52°N), with the goal of corroborating biomarker SST measurements from ~13 to 4.5 Ma. My data indeed corroborate the cooling trends shown by biomarker data from recent studies on samples from Site 982; however, water temperature values computed from stable isotope values were, on average, cooler than those estimated by alkenone temperature records, likely due to differing biology of planktonic foraminifera and alkenone-producing coccolithophores.

ACKNOWLEDGEMENTS

I would like to thank Ken Miller for providing me with the opportunity to conduct this research, especially under such short notice and strange circumstances. I came into grad school believing I knew exactly what direction I wanted to take my scientific career, but you and your lab have completely changed my trajectory for the better. Thank you, as well, for your endless patience in the face of my penchant for tardiness.

A massive thank you to Masha Makarova, whose ability to simultaneously be an incredible teacher, mentor, friend, dance partner, drinking buddy, and chef will never cease to amaze me. Thanks for helping me through some of the rougher parts of my grad school experience and for being there for so many of the best parts, too.

Thank you to Jim Wright for encouraging me to apply to Rutgers so late in the summer of 2017 and for facilitating the entire process. Thank you, as well, for looking at my samples so many times to help me figure out what the heck I was dealing with.

Thank you to Jim Browning for agreeing to be on my committee when I asked without warning, and for saving me from being secluded in WL 281 by spearheading the effort to turn the back room into the picking room.

Thank you to Rick Mortlock, Mark Yu, and Aaron Watters for eternally wrestling with the mass spectrometer in order to get data to me (and everyone else) as quickly as possible, despite all of the obstacles that thing throws at you.

Finally, thanks to Ronan Keating for picking and sonicating so many of my samples during your first few weeks in the lab even though your sample order was on the way, and thanks for taking up the helm of 982B stable isotope work.

TABLE OF CONTENTS

LIST OF FIGURES

all of pores in **D** are devoid of nannofossils, but that the pores in **D** are clearer relative to those in **A** and **B**.

Figure 7. A) The age model created for this study (Jansen et al., 1996; ODSN, 2011; Gradstein et al., 2012). The highlighted portion of the x-axis marks the age range of samples used in this study. **B)** A comparison of the age model created for this study, and the age model used by Andersson and Jansen (2003) (black line). Highlighted FAD and LAD data show the differences in the first and last appearance data used in each study. The equations for each interval can be found in **Table 3**.

Figure 8. Stable oxygen isotope data (**Table 4**) from this study. These values decrease from the late Middle Miocene through the latest Late Miocene. The values briefly increase at the beginning of the earliest Early Pliocene, then decrease once again.

Figure 9. Stable carbon isotope data (**Table 4**) from this study. **A)** Isotope record from planktonic species. Note that the data from *G. bulloides* varies across a relatively large range of $\delta^{13}C$ values. This variability is likely due to the tendency of *G. bulloides* in the North Atlantic to bloom during peak springtime algal blooms (Wolfteich, 1994). **B)** Isotope record from benthic species. The data from these two species correspond very well, relative to the planktonic data.

Figure 10. Water temperature values (**Table 5**) computed from $\delta^{18}O$ values (**Fig. 8**) and $\delta^{18}O_{seawater}$ after Cramer et al. (2011). Both planktonic and benthic species indicate a

cooling trend throughout the majority of this timeframe. The magnitude of this cooling markedly increased in the latest Late Miocene. Temperatures began to rise again during the latest Late Miocene and into the earliest Early Pliocene, though the youngest samples indicate that temperatures began to drop again shortly after this rise.

List of Tables

Table 5. Temperature values calculated from $\delta^{18}O$ values using the methodology outlined in **Stable isotope analyses** (Kim and O'Neil, 1997; Cramer et al., 2011). These data are plotted in **Fig.1.**

INTRODUCTION

Ocean circulation plays a major role in the redistribution of heat energy around the Earth from the warmer equatorial regions to the colder poles. A host of evidence indicates that global climate change and ocean circulation have been intimately related throughout the Cenozoic Era (~66.4 Ma to the present) (e.g., Zachos et al., 2001). Cenozoic climate trends are reflected in $\delta^{18}O$ values measured from planktonic and benthic foraminiferal fossils (Savin et al., 1985; Miller and Katz, 1987; Wright and Miller, 1993; 1996; Pagani et al., 1999; Zachos et al., 2001; Woodard et al., 2014; Abelson and Erez, 2017). At the beginning of the Cenozoic, the global climate was quite warm relative to the climate of the modern day (Zachos et al., 2001; Boyle et al., 2017). Stable isotope records show that average global temperatures increased into the Early Eocene Climate Optimum (EECO, ~50 Ma), after which the Earth experienced a long-term cooling (Miller et al., 1987).

Production of deepwater in the Atlantic has varied greatly throughout the Cenozoic in terms of the source, geochemical properties, and circulation path of deep-water masses (Miller and Katz, 1987; Wright and Miller, 1993; 1996; Hohbein et al., 2012; Woodard et al., 2014; Abelson and Erez, 2017). Today, the thermohaline cycle is controlled by density-driven deep-water production in the North Atlantic and the Southern Ocean (Morozov et al., 2010). In the North Atlantic, water from the Nordic Seas, the Labrador Sea, the Mediterranean Sea, and the Southern Ocean (Morozov et al., 2010) combine to form a salty, low-nutrient deep-water mass known as North Atlantic Deep Water (NADW) (Worthington, 1976). The majority of the water that contributes to NADW forms north of the Greenland-Scotland Ridge (GSR) in the Norwegian-

Greenland Sea and flows out through shallow gateways (**Fig. 1**) (Wright and Miller, 1996; Hohbein et al., 2012; Boyle et al., 2017). A more generalized term, Northern Component Water (NCW), is used to describe low-nutrient bottom water analogous to NADW that once flowed from north of the GSR but may not necessarily have had the specific geochemical properties used to define NADW today (Miller and Katz, 1987; Wright et al., 1991).

From as early as the Eocene (Poore et al., 2009) to the present day, the height of the GSR may have had a dramatic effect on the flow of NCW and NADW (Wright and Miller, 1996). Specifically, the depth of the Denmark Strait and the Faroe-Shetland Channel has affected NCW outflow since at least the Middle or Late Miocene (~12-5 Ma) (Poore et al., 2009). Changes in the temperature of the mantle plume below Iceland have caused the height of the GSR to vary by up to 200 m over time, more than enough of a change to greatly affect the ability of NCW or NADW to flow through the Faroe-Shetland Channel and Denmark Strait into the Atlantic basin (Wright et al., 1991; 1992; Wright and Miller, 1993; 1996; Poore et al., 2009).

The waters of the modern-day Southern Ocean surround Antarctica and flow primarily via the Antarctic Circumpolar Current (ACC; Morozov et al., 2010; Abelson and Erez, 2017). Deep water is formed in the Weddell Sea; this water is less salty, but colder and denser than NADW and is known as Antarctic Bottom Water (AABW) (Morozov et al., 2010). Southern Component Water (SCW) is the generalized term for deep water that once formed in the Antarctic but did not necessarily have the specific geochemical properties used to define AABW today (Miller and Katz, 1987; Wright et al., 1991; 1992; Wright and Miller, 1993; 1996). AABW flows northward from the ACC into the Atlantic, Pacific, and Indian Oceans (Wright et al., 1991; 1992; Wright and Miller, 1993; 1996; Morozov et al., 2010). Since the Oligocene, both NCW and SCW have played dominant roles in global deep-water circulation, with fluxes in NCW production often determining the range of SCW circulation in the Atlantic (Wright et al., 1991; 1992; Wright and Miller, 1993; 1996; Abelson and Erez, 2017; Boyle et al., 2017).

Neogene surface water circulation

Around the Eocene-Oligocene transition (EOT, ~33.7 Ma), a shallow proto-ACC began to develop (Scher and Martin, 2006; Scher et al., 2015; Abelson and Erez, 2017). Neodymium isotope ratios from sediments from Ocean Drilling Program (ODP) Site 1090 indicated that the Southeast Pacific and South Atlantic converged around 41 Ma suggesting that the Drake Passage started to form around that time (Scher and Martin, 2006). Similarly, neodymium isotope ratios from sediments from ODP Sites 1124, 1168, and 1172 indicated that the Indian and Pacific Oceans converged around 33.5 Ma, suggesting that the Tasman Gateway opened up by around that time (Scher et al., 2015). The opening of both of these passages created a circuit through which the proto-ACC could flow (Scher and Martin, 2006; Scher et al., 2015; Abelson and Erez, 2017). This current prevented warmer surface waters from lower latitudes from circulating towards Antarctica (Abelson and Erez, 2017). With the loss of warmer water input combined with long-term decrease in atmospheric CO_2, the waters around Antarctica grew progressively colder (Abelson and Erez, 2017). While the Southern Ocean cooled, the North and South Atlantic experienced little to no change in water temperature, based on $\delta^{18}O$ records (Abelson and Erez, 2017).

Benthic foraminiferal records indicate that throughout the Early Miocene (~22-16 Ma) SSTs warmed in the Atlantic, Pacific, and Indian Oceans (Savin et al., 1985), with temperatures peaking during the Miocene Climate Optimum (MCO, 17-14.8 Ma; Zachos et al., 2001). Throughout this time interval, Antarctic ice sheets remained quite small, though they experienced a period of minor growth during the Mi2 glaciation (ca. 16.2 Ma, Miller et al., 1991). During the early Middle Miocene Climate Transition (MMCT, ca. 14.8-12.8 Ma), a permanent East Antarctic Ice Sheet developed (Miller et al., 1991). At this time, Atlantic SSTs apparently changed asymmetrically: waters in the northernmost Atlantic, as well as the eastern equatorial Atlantic, apparently cooled, while the SSTs in most of the South Atlantic remained warm (Savin et al., 1985; Super et al., 2018). In fact, surface waters off the coast of South Africa warmed even further (Savin et al., 1985). During the Late Miocene Cooling (LMC, ca. 8-6 Ma), the North Atlantic apparently cooled dramatically (Herbert et al., 2016).

The driving forces behind the highly variable SSTs throughout the Miocene have been long debated (Pagani et al, 1999; Herbert et al., 2016; Super et al., 2018). Among the possible causes of this variation are changes in the amount of carbon dioxide in the atmosphere (pCO_2) and shifts in the magnitude of meridional heat transport via deep-water circulation (Savin et al., 1985; Pagani et al., 1999; Herbert et al., 2016; Super et al., 2018). Based on alkenone records from Deep Sea Drilling Project (DSDP) Site 608 in the North Atlantic, Pagani et al. (1999) suggested that changes in pCO_2 were neither the cause of late Early Miocene warming or late Middle to Late Miocene cooling; therefore, Pagani et al. (1999) asserted that ocean circulation was the cause of the Miocene temperature shifts. However, Herbert et al. (2016) suggested, based on alkenone records from sites around the globe, that at least the cooling in the Late Miocene was the result of reduced pCO_2. Additionally, Super et al. (2018) sought to rectify SST estimates from DSDP Site 608 made by Pagani et al. (1999) using biomarker ($U^{k'}_{37}$ and TEX_{86}) temperature proxies on the same samples used by Pagani et al. (1999). Super et al. (2018) also concluded that Miocene pCO_2 values were more variable than the results of Pagani et al. (1999) had suggested. Thus, changes in pCO_2 were indeed likely the force that drove Miocene SST variability (Herbert et al., 2016; Super et al., 2018).

The relatively cool North Atlantic SSTs of the Late Miocene began to rise again in the Early Pliocene (Lawrence et al., 2009; Herbert et al., 2016). Alkenone records from Site 982 show warming at ~4 Ma and an overall trend towards colder temperatures beginning at ~3.5 Ma, likely due to reduced pCO_2 (Lawrence et al., 2009). This cooling trend allowed for ice sheet growth in the Arctic and caused an especially rapid drop in SSTs from ~3.5 to 2.5 Ma (Lawrence et al., 2009). After 2.5 Ma, the global cooling trend continued, but at a slower rate, resulting primarily in ice sheet growth in the Northern Hemisphere, rather than further decrease in SSTs, ushering in the glacial-interglacial cycles of the Pleistocene and Holocene (Lawrence et al., 2009).

Neogene deep-water circulation

During the Middle and Late Miocene, changes in Northern Hemisphere ice volume caused fluxes in bottom water production in the North Atlantic (Miller and Katz, 1987; Wright et al., 1991; Wright and Miller, 1993). Also during the Miocene, deep water from the North Atlantic flowed to Antarctica, where it upwelled and evaporated;

this moisture was eventually incorporated into Antarctic ice sheets, promoting the growth of a permanent Antarctic glacier (Wright and Miller, 1996).

In the Early Miocene, global deep-water circulation was dominated by a mixture of SCW with minor inputs from NCW and waters flowing out of the Tethys Ocean, as revealed by foraminiferal $\delta^{18}O$ and $\delta^{13}C$ records (Wright and Miller, 1993). Low production of NCW allowed for shallow-depth deposition of carbonate sediments to occur at the Newfoundland Ridge and farther south along the North American continental margin (Boyle et al., 2017). However, around 22-20 Ma, a brief period of global cooling resulted in an increased rate of NCW production, leading to the erosion and dissolution of the tops of many of the sediment drifts that had been deposited in the Late Oligocene and Early Miocene (Miller and Katz, 1987; Boyle et al., 2017). Between 19.5 and 16 Ma, NCW production continued to increase, possibly due to inputs of salty water to the North Atlantic from the closing Tethys Ocean (Wright et al., 1991; 1992); NCW reached peak production around 17 Ma, according to $\delta^{13}C$ records (Wright and Miller, 1996).

By 12.5 Ma, $\delta^{13}C$ records reveal that the rate of NCW production had increased once again and would remain as the dominant deep-water mass in terms of global circulation for the remainder of the Miocene (Wright and Miller, 1993; 1996). Geochemical properties of benthic foraminiferal fossils indicate that deep circulation in the Atlantic was similar to that of the modern Atlantic at this time (Wright and Miller, 1996). NCW, warmer and less dense than the water masses formed in the Southern Ocean, began to upwell as it flowed as far south as Antarctica (Wright and Miller, 1996). A second large-scale erosional event—similar to the one in the Early Miocene—occurred between 11-10 Ma, resulting in another depositional hiatus (Miller and Katz, 1987). $\delta^{13}C$

records from the Southern Ocean reveal that between 9.8 and 9.3 Ma, 50-90% of Southern Ocean deep water by volume was derived from NCW (Wright et al., 1991). However, between 9.2 and 8.6 Ma, a "complete shutdown" of NCW production allowed SCW to occupy most of the deep North Atlantic (Wright et al., 1991). By 7 Ma, NCW production had resumed, and NCW once again flowed to the Southern Ocean (Wright et al., 1991). Fluxes in bottom-water production during the Middle and Late Miocene were likely linked with changes in Northern Hemisphere ice volume, based on $\delta^{18}O$ records (Miller and Katz, 1987; Wright et al., 1991; Wright and Miller, 1993). Wright et al. (1991) and Poore et al. (2009) credit changes in NCW production to the thermal uplift and subsidence of the Faroe-Shetland Channel throughout the Miocene.

Throughout the Pliocene, the rate of NCW production and outflow from north of the GSR was largely controlled by the depth of the Denmark Strait and glacial-interglacial cycles (Wright et al., 1992; Wright and Miller, 1996; Poore et al., 2009). Based on changes in the bathymetry of the GSR known from seismic imaging, the Denmark Strait was relatively deep between 5 and 3 Ma, allowing for a more substantial outflow of NCW (Poore et al., 2009). Boyle et al. (2017) state that it was at this time that the "establishment of modern deep circulation in the North Atlantic" had occurred. After 3 Ma, $\delta^{18}O$ records indicate that fluctuations in NCW production occurred as a result of the growth and contraction of Northern Hemisphere ice sheets (Raymo et al, 1992; Wright and Miller, 1996). The production of NCW decreased during glacial intervals and increased during interglacials (Wright and Miller, 1996). When NCW was strengthened, the production of SCW increased, as well (Woodard et al., 2014). Based on decreased rates of opal accumulation in the Antarctic, primary production in the ACC declined around 2.73 Ma; Woodard et al. (2014) credit this decline to a reduction of mixing in the ACC. As such, heat from warmer NCW was unable to efficiently be exchanged with cooler SCW, resulting in colder Antarctic waters, and an intensification of SCW production (Woodard et al., 2014). With a greater input volume of SCW, water in the ACC became more similar to SCW than NCW in terms of $\delta^{18}O$ and $\delta^{13}C$ values (Woodard et al., 2014). Subsequently, bottom water that was circulated throughout the Pacific and Indian Oceans—and to a lesser extent, the Atlantic Ocean—became more chemically similar to SCW (Woodard et al., 2014).

Middle and Late Miocene Atlantic planktonic foraminiferal distribution

In the Middle Miocene, the tropical-subtropical foraminifer province, dominated by *Globigerinoides ruber* and *Globorotalia menardii*, was generally restricted to between 15°S and 15°N latitude (Thunell and Belyea, 1982). This range was markedly smaller than the tropical-subtropical province of the warmer Early Miocene (Thunell and Belyea, 1982). The transitional province, marked by the coexistence of *Globigerina bulloides*, *Globigerinita glutinata*, and *Globorotalia scitula*, stretched from 25 to 65°N, and 20 to 65°S (Thunell and Belyea, 1982). A mix of tropical-subtropical and transitional species coexisted between ranges of these provinces (Thunell and Belyea, 1982). Above 65°N and 65°S latitude, the polar-subpolar species *Neogloboquadrina pachyderma* (dextral and sinistral) dominated (Thunell and Belyea, 1982). Through the Middle Miocene, the range of polar-subpolar species expanded towards lower latitudes, particularly in the North Atlantic as high-latitude water masses spread towards the equator (Thunell and Belyea, 1982). An eastern boundary current brought polar-subpolar species as far south as 50°N in the eastern Atlantic, while these species in the western northern Atlantic were generally restricted to above 65°N (Thunell and Belyea, 1982).

The Late Miocene saw an expansion of tropical-subtropical and polar-subpolar provinces, at the expense of transitional provinces (Thunell and Belyea, 1982). The more marked expansion was that of polar-subpolar province, which reached as far south as 10°N latitude in the North Atlantic and was dominated by the species *Neogloboquadrina pachyderma* (dextral and sinistral), *Globigerina bulloides*, and *Globorotalia glutinata* (Thunell and Belyea, 1982). The tropical-subtropical assemblage contained the species *Sphaeroidinellopsis semiluna*, *Sphaeroidinellopsis subdehiscens*, *Globoquadrina altispira*, and *Orbulina universa*, and the transitional province was marked by the coexistence of *Globorotalia dehiscens*, *Globigerina nepenthes*, and *Sphaeroidinellopsis subdehiscens* (Thunell and Belyea, 1982). Thunell and Belyea (1982) emphasize the large overlap among all provinces across this time interval, owing to migrations of all three assemblages as ocean temperatures fluctuated throughout the Late Miocene.

Oceanographic setting

Rockall Plateau is a shallow (~1000 m below the sea surface) continental fragment or microcontinent (Roberts and Deacon, 1975; Jansen et al., 1996) ~480 km off the western coast of Scotland (Ryan et al., 2009). Only a small portion of the plateau— Rockall Island— sits above the sea surface; the rest of the plateau is submerged (Roberts and Deacon, 1975; Jansen et al., 1996). On the plateau, Cenozoic limestones, carbonate oozes, and cherts overlay Laxfordian and Grenvillian granulites (Roberts and Deacon, 1975). Site 982 was drilled as part of the Ocean Drilling Program (ODP) Leg 162

(57°30.992'N, 15°52.001'W) in 1134 m water depth (Jansen et al., 1996). The site is located in a bathymetric depression in the plateau known as the Hatton-Rockall basin (Jansen et al., 1996). This basin is surrounded by sediment banks, which may have been the source of the various foraminiferal turbidite successions found within the cores from this site (Jansen et al., 1996).

In the modern-day, summer water temperatures near Site 982 range from ~14.6°C at the surface to ~4.75°C near the seafloor (**Fig. 2**; Reid and Mantyla, 1994). The surface mixed layer is virtually absent—save for in the spring (Wolfteich, 1994)— and the thermocline is quite shallow, situated in the upper ~50 m of the water column (Reid and Mantyla, 1994). Below the thermocline is a thick (~650 m) layer of ~9°C mode water (Reid and Mantyla, 1994). Deep-water temperatures below the layer of mode water range from ~8.5°C directly below the mode water layer to ~4.75°C at the seafloor (Reid and Mantyla, 1994).

Objectives of this thesis

The purpose of this thesis is to reconstruct the history of the North Atlantic SSTs at and around Site 982 from ~12 to 5 Ma by measuring planktonic foraminiferal stable isotope records ($\delta^{18}O$ and $\delta^{13}C$). Oxygen isotope records act as a proxy for water temperature at different depths in the water column. Similarly, carbon isotope records act as a proxy for the apparent oxygen utilization at different depths in the water column. This research is part of a larger project that investigates the evolution of northern deep waters in terms of SST, thermocline structure, and meridional thermal gradients in the North Atlantic subtropical and subarctic gyres, and changes in biogeochemical cycling and biogenic production through the Miocene and into the Paleogene. As such, the results of this study can be compared with studies from DSDP Sites 608, 558, and 563, that, in addition to Site 982, are part of the Miocene Western North Atlantic transect (WNAT) (**Figs. 3** and **14**) (Makarova et al., 2018).

METHODS

Sample preparation and picking

One hundred and thirty-four core samples from depths of 131.2 mbsf to 418.2 mbsf were taken at a resolution of ~2 meters by the Bremen Core Repository (**Table 1**). Samples were disaggregated in a sodium metaphosphate solution (5.5 g of sodium metaphosphate per liter of water) to deflocculate clays. The samples were then washed through a 63-μm sieve to separate the fine fraction (<63 μm). The >63 μm fraction was dried overnight in a 50°C oven and weighed dry to compute the percentage of coarse sediment (**Fig. 4**; **Table 2**). For stable isotope analysis of planktonic foraminifera, specimens of *Orbulina universa* (*O. universa*, **Fig. 5A**) and *Globigerina bulloides* (*G. bulloides*; **Fig. 5B**-**C**) were picked using the taxonomy of Kennett and Srinivasan (1983). For stable isotope analysis of benthic foraminifera, specimens of *Cibicidoides mundulus* (*C. mundulus*; **Fig. 5D**-**E**) and *Planulina wuellerstorfi* (*P. wuellerstorfi*; **Fig. 5F**-**G**) were picked using the taxonomy of Holbourn et al. (2013). Seven to ten individuals of each species were chosen from most samples, with a minimum of three individuals chosen in order to avoid seasonal signal. Specimens were mostly picked from size fraction of 250-355 μm, with a minimum size of 212 μm in order to exclude juvenile individuals. All specimens were cleaned in a Sonicator for ~12 seconds in order to remove calcareous nannofossils stuck to the tests (**Fig. 6**). Images of one well-preserved specimen of each species were captured with a scanning electron microscope (**Fig. 5**).

Age model and sedimentation rates

An age-depth plot (**Fig. 7A**) was created using first appearance data (FADs) and last appearance data (LADs) from planktonic foraminifer, calcareous nannofossil, diatom, and silicoflagellate species listed in Jansen et al. (1996). Foraminifer and nannofossil ages from Jansen et al. (1996) were converted to ages from the Geological Time Scale 2012 (GTS2012; Gradstein et al., 2012). Species of foraminifera that were listed in Jansen et al. (1996) but not in GTS2012 were excluded from the plot. Ages for diatom and silicoflagellate species listed in Jansen et al. (1996) were converted using the Ocean Drilling Stratigraphic Network age converter (ODSN, 2011), as these groups were not mentioned in GTS2012.

A visual best-fit line was drawn onto the age-depth plot (**Fig. 7A**, dashed orange line) in order to determine the ages of the samples used in this study, as well as to calculate sediment deposition rates at the site from 20 Ma to the present. The best-fit line was drawn such that it agreed with as many FADs and LADs as possible. The model was split into four different intervals, with one major hiatus marked by a turbidite sequence within the core (Jansen et al., 1996). The equations used to convert depth in mbsf (x) to age in Ma (y) for each of these intervals, as well as the sedimentation rates associated with each interval can be found in **Table 3**.

The majority of the species included in the plot align along or near the best-fit line. Some species, such as the coccolithophore *Cyclicargolithus floridanus*, did not fit this line well, possibly due to diachrony. Two LADs listed in GTS2012— those of the planktonic foraminifera *Neogloboquadrina acostaensis* and *Catapsydrax dissimilis*— were relatively far from the best-fit line. As such, in the case of the LAD of *Neogloboquadrina acostaensis*, both the age from Jansen et al. (1996) and the age from GTS2012 were included in the plot, though only the former was considered when creating the best-fit line. The difference in the LADs of *Neogloboquadrina acostaensis* may be the fact that the LAD reported by Jansen et al. (1996) is based on sediments from the North Atlantic (Site 982) and the LAD listed in GTS2012 is based on sediments from the South Atlantic. In the case of the LAD of *Catapsydrax dissimilis*, Jansen et al. (1996) and GTS2012 offer relatively disparate ages, as well. As such, the age of the LAD of *Catapsydrax dissimilis* was determined using a recalibrated age-depth relationship, based on GTS2012, from DSDP Site 608 (Baldauf et al., 1987) using magnetobiostratigraphic calibrations from Miller et al. (1991). From this relationship, the age of the LAD of *Catapsydrax dissimilis* was extrapolated to be ~17.8 Ma, implying that the age of this datum in GTS2012 is slightly too old. Only the recalibrated age from Site 608 was considered when creating the best-fit line, though the original age from GTS2012 was included in the plot, as well.

The age model created by Andersson and Jansen (2003) (**Fig. 7B**) covered a significantly shorter age range than the age model created for this study. The age range of the model by Andersson and Jansen (2003) roughly correlates to the range covered by **Equation 2** (**Table 3**). Only nannoplankton first and last appearance data were included in the age model by Andersson and Jansen (2003), and the ages used in said model were derived from Jansen et al. (1996). As such, there is a relatively large (~1 Ma) offset between the two age models.

Stable isotope analyses

The ratio of oxygen isotopes (^{16}O and ^{18}O, or $\delta^{18}O$; **Fig. 8**; **Table 4**) in calcium carbonate ($CaCO_3$) that the foraminiferal tests are composed of were used to estimate the temperatures of the water the foraminifera lived and grew in. Similarly, analyses of the ratio of stable isotopes of carbon (^{12}C and ^{13}C, or $\delta^{13}C$; **Fig. 9**; **Table 4**) in the calcium carbonate were used as a proxy for the apparent oxygen utilization at different depths in the water column. Using a Micromass Optima Mass Spectrometer with an attached multi-prep device, stable isotope analyses were conducted on the tests of individuals of each of the studied species. Carbonate samples were reacted in 100% phosphoric acid (H_3PO_4) at 90°C for 15 minutes and the evolved CO_2 gas was collected in a liquid nitrogen cold finger. Stable isotopes ratios are reported in standard delta notation in parts per thousand, relative to Vienna-Pee Dee Belemnite ($\delta^{18}O_{VPDB}$ and $\delta^{13}C_{VPDB}$), and are calculated as follows:

$$\delta^{18}O = [(R_{O\ sample} / R_{O\ standard}) - 1] \times 1000$$

$$\delta^{13}C = [(R_{C\ sample} / R_{C\ standard}) - 1] \times 1000$$

in which R_O is $^{18}O/^{16}O$, and R_C is $^{13}C/^{12}C$. One-sigma analytical errors based on analyses of an internal laboratory reference material (~8 standards for every 24 samples) are

$\pm$ 0.08 ‰ and $\pm$ 0.05 ‰ for $\delta^{18}O$ and $\delta^{13}C$, respectively (**Table 4**). Water temperature values (**Fig. 10**) were computed from $\delta^{18}O$ values using the following formula from Kim and O'Neil (1997):

$$T = 16.1 - 4.64(\delta^{18}O_{foram} - \delta^{18}O_{seawater}) + 0.09(\delta^{18}O_{foram} - \delta^{18}O_{seawater})^{2}$$

in which T is temperature in °C. $\delta^{18}O_{seawater}$ values from Cramer et al. (2011) (**Fig. 11**; **Table 5**) were used for these temperature calculations. Cramer et al. (2011) used Pacific benthic foraminiferal Mg/Ca records as a proxy for water temperature, sea level records as a proxy for ice volume, and $\delta^{18}O$ records from benthic foraminifera (expressed relative to the Vienna Pee Dee Belemnite standard, VPBD) as a proxy for both sea water temperature and ice volume in order to constrain $\delta^{18}O_{seawater}$ values (expressed relative to Vienna Standard Mean Ocean Water, VSMOW). As such, the $\delta^{18}O_{seawater}$ values from Cramer et al. (2011) do not account for local causes of $\delta^{18}O_{seawater}$ variation such as mixing, evaporation, and precipitation.

RESULTS

Impact of vital effects on planktonic stable isotope values

Though the $\delta^{13}C$ and $\delta^{18}O$ values of planktonic foraminifera are indicative of the $\delta^{13}C$ and $\delta^{18}O$ values of the seawater in which the organisms lived and grew, they are not simply an exact reflection of the $\delta^{13}C$ and $\delta^{18}O$ values of the ambient seawater, they are more so reflections of a combination of environmental factors (Spero et al., 1997; Bijma et al., 1999; Bemis et al., 2000). Factors such as ocean alkalinity (Spero et al., 1997) and an individual's cellular respiration can affect both the $\delta^{13}C$ and $\delta^{18}O$ values of planktonic foraminiferal tests (Bijma et al., 1999; Bemis et al., 2000). Increased seawater alkalinity—specifically an increased concentration of carbonate ions (CO_3^{2-})—decreases the $\delta^{13}C$ and $\delta^{18}O$ of carbonate shells formed in said seawater (Spero et al., 1997). Additionally, an individual's cellular respiration can cause the water immediately surrounding said individual to become more acidic (via the release of CO_2), leading to an effect counter to that of increased ocean alkalinity (Bijma et al, 1999; Bemis et al., 2000).

For *O. universa* specifically, light intensity throughout an individual's growth can influence the individual's $\delta^{13}C$ values (Spero and DeNiro, 1987; Bijma et al., 1999). In more intense light causes *O. universa* tests produce higher $\delta^{13}C$ values because the species has photosynthetic symbionts (zooxanthellae) that preferentially sequester light ^{12}C during photosynthesis; to an extent, increased light intensity begets an increase in photosynthesis, leading to higher foraminiferal $\delta^{13}C$ values (Spero and DeNiro, 1987; Bijma et al., 1999).

Abundant in nearly all samples analyzed for this study, *G. bulloides* produced the widest range of stable isotope values relative to the other three species used in this study, with stark changes in $\delta^{13}C$ and $\delta^{18}O$ over relatively short periods of time (**Figs. 8-10**). Both the wide range of $\delta^{13}C$ and $\delta^{18}O$ values and the apparent rate of change in $\delta^{13}C$ and $\delta^{18}O$ values are likely due to vital effects related to the scale and seasonal nature of *G. bulloides* blooms (Wolfteich, 1994). In the North Atlantic, springtime algal blooms coincide with the maximum planktonic foraminiferal flux, with *G. bulloides* accounting for the majority of this flux (Wolfteich, 1994). *G. bulloides* typically occupies the surface mixed layer that forms above the thermocline in the North Atlantic as the result of springtime winds (Fairbanks et al., 1982).

Assuming this behavior was also exhibited by *G. bulloides* in the Miocene and Pliocene, the majority of the preserved individuals likely lived and died during the late spring through early summer. As such, *G. bulloides* $\delta^{18}O$ values are likely representative of mixed layer water temperatures during the spring. Some $\delta^{18}O$ values of *G. bulloides*, however, were lower than (and calculated water temperature values were warmer than) those from *O. universa* reported at the same given age. Additionally, the accumulation of organic carbon from large springtime algal blooms that coincide with *G. bulloides* blooms (Wolfteich, 1994) may have caused anomalously low $\delta^{13}C$ values; the magnitude of this vital effect could possibly correlate to bloom size, with larger algal blooms skewing $\delta^{13}C$ values to a greater extent. Bemis et al. (2000) also found that at high metabolic rates, *G. bulloides* incorporate more respired CO_2 into their tests, which can cause test $\delta^{13}C$ values to decrease by up to 0.11‰.

Oxygen isotopes

The planktonic $\delta^{18}O$ record was quite variable relative to the range of benthic $\delta^{18}O$ values (**Fig. 8**). The $\delta^{18}O$ record obtained from *O. universa* varied from as isotopically low as 0.45‰ (12.69 Ma) to as isotopically high as 2.05‰ (5.53 Ma). The $\delta^{18}O$ record obtained from *G. bulloides* varied from as isotopically low as 0.38‰ (11.55 Ma) to as isotopically high as 1.90‰ (6.63 Ma). Between ~13 Ma and ~11.5 Ma, *O. universa* and *G. bulloides* $\delta^{18}O$ values were fairly disparate and variable; however, between 11.5 Ma and the beginning of the hiatus (10.25 Ma), *O. universa* and *G. bulloides* $\delta^{18}O$ values tracked much closer to one another and gradually trended towards heavier values.

From the end of the hiatus (8.91 Ma) until ~5.5 Ma, *O. universa* $\delta^{18}O$ values ranged over ~0.85‰ and *G. bulloides* $\delta^{18}O$ values ranged over ~1.35‰; $\delta^{18}O$ values from both *O. universa* and *G. bulloides* increased on average during this interval. At 5.53 Ma, $\delta^{18}O$ values from *O. universa* reached the maximum for the analyzed interval, at 2.05‰. Similarly, at 5.53 Ma $\delta^{18}O$ values from *G. bulloides* were quite high, recording a value of 1.85‰. After this high point, *O. universa* $\delta^{18}O$ values dropped by 0.86‰ by 5.10 Ma and *G. bulloides* $\delta^{18}O$ values dropped by 0.93‰ by 4.76 Ma. The $\delta^{18}O$ values of both planktonic species rose again after this short period of warming.

Overall, the benthic foraminiferal $\delta^{18}O$ record spanned a much more confined range of values, dropping to 1.88‰ at its lowest (7.74 Ma), and rising to 2.73‰ at its heaviest (5.53 Ma). Benthic $\delta^{18}O$ values never rose above planktonic $\delta^{18}O$ at any given time. Prior to the hiatus (10.25 Ma), benthic values largely remained at 2 ± 0.25‰. After the hiatus (8.91 Ma) and until ~6 Ma, *P. wuellerstorfi* $\delta^{18}O$ values fluctuated between 2‰ and 2.5‰. Between 6 Ma and 5.52 Ma, *P. wuellerstorfi* $\delta^{18}O$ values indicate that deep water rapidly became colder, just as *O. universa* and *G. bulloides* $\delta^{18}O$ values indicated for the surface waters. *P. wuellerstorfi* $\delta^{18}O$ values also began to rise again after hitting this low point, dropping to 2.06‰ by 4.76 Ma.

Temperature values

Temperature values computed from both planktonic $\delta^{18}O$ values indicate a cooling trend throughout the majority of the interval covered in this study (**Fig. 10**). The magnitude of this cooling markedly increased in the latest Late Miocene. Temperatures began to warm during the latest Late Miocene and into the earliest Early Pliocene, though the youngest samples indicate that temperatures began to drop again shortly after this period of warming. SSTs decreased relatively steadily from 14.2°C at 12.69 Ma to 9.4°C at 10.37 Ma. Shortly after the hiatus (8.91 Ma), $\delta^{18}O$ values from *G. bulloides* indicate that water temperatures peaked, rising as high as 15.5°C at 8.68 Ma. $\delta^{18}O$ values from *O. universa* suggest that water temperatures took a bit longer to peak, reaching 14.2°C at 8.00 Ma. Temperatures in the upper water column decreased to between 7.7°C and 8.3°C by 5.53 Ma. $\delta^{18}O$ values from *O. universa* indicate that the upper water column warmed to 10.9°C by 5.10 Ma but cooled to 8.9°C by 4.55 Ma. Similarly, $\delta^{18}O$ values from *G. bulloides* indicate that these waters warmed, rising to 12.4°C by 4.76 Ma and then cooled to 9.9°C by 4.55 Ma.

Unlike water temperatures nearer to the surface, deep-water temperatures remained fairly stable prior to the hiatus (10.25 Ma). Temperatures computed from *P. wuellerstorfi* and *C. mundulus* $\delta^{18}O$ values indicate that deep-water temperatures generally remained around 7 ± 0.5°C; the temperatures computed from *P. wuellerstorfi* $\delta^{18}O$ values indicate a rise to ~9°C between 11.01 Ma and 10.79 Ma. From the end of the hiatus (8.91 Ma) until at least 6.53 Ma, deep-water temperatures fluctuated between ~6°C and ~8°C. After this relatively stable period, deep-water temperatures rapidly dropped to 4.6°C by 5.59 Ma. The temperatures then began to rise again, reaching 7.4°C by 4.83 Ma.

Carbon isotopes

As was the case with $\delta^{18}O$ values, the planktonic $\delta^{13}C$ record (**Fig. 9A**) was quite variable relative to the range of benthic foraminiferal $\delta^{13}C$ values (**Fig. 9B**). $\delta^{13}C$ values from *O. universa* varied from as low as 0.40‰ (6.38 Ma) to as high as 2.15‰ (7.26 Ma).

From at least 12.69 Ma until 7.26 Ma, *O. universa* $\delta^{13}C$ values cycled between peaks near 2 ± 0.25‰ and troughs near 1.5 ± 0.25‰, with each cycle lasting ~0.5 Myr. After 7.26 Ma, $\delta^{13}C$ values began to fluctuate between ~0.5‰ and ~1.5‰, with three peaks at 1.35 ± 0.1‰, and three troughs at 0.6 ± 0.2‰, with more variable cycle lengths (~0.25 to ~1 Myr) than the cycles prior 7.26 Ma. $\delta^{13}C$ values from *G. bulloides* varied from as low as -0.59‰ (5.53 Ma) to as high as 1.61‰ (8.00 Ma). From 12.69 Ma until the beginning of the hiatus (10.25 Ma), most *G. bulloides* $\delta^{13}C$ values fell between 0.5‰ and 1‰, with a few short periods of anomalously low or high values. After the hiatus (8.91 Ma) until 7.86 Ma, $\delta^{13}C$ were especially variable, ranging from -0.12‰ to 1.61‰. Between 7.86 Ma and 6.63 Ma, *G. bulloides* $\delta^{13}C$ values were their most stable, with almost all measurements falling between 0.5‰ and 1‰. After this stable interval, *G. bulloides* $\delta^{13}C$ values dropped rapidly, reaching -0.59‰ by 5.53 Ma. This decrease was followed by another period of fluctuating $\delta^{13}C$ values, increasing by 1.15‰ by 5.35 Ma, falling by 0.85‰ by 5.02, and rising again by 0.48‰ by 4.55 Ma.

Overall, the benthic foraminiferal $\delta^{13}C$ record spanned a much more confined range of values, almost all falling between 0.5‰ and 1.5‰. After the hiatus (8.91 Ma) until ~6 Ma, *P. wuellerstorfi* $\delta^{13}C$ values fluctuated between 2‰ and 2.5‰. Between 6 Ma and 5.52 Ma, *P. wuellerstorfi* $\delta^{13}C$ values indicate that deep water rapidly became isotopically heavier, just as *O. universa* and *G. bulloides* $\delta^{13}C$ values indicated for the water in the upper water column. *P. wuellerstorfi* $\delta^{13}C$ values also began to become isotopically heavier after hitting this low point, dropping to 2.06‰ by 4.76 Ma.

Both the planktonic and the benthic $\delta^{13}C$ records capture the late Miocene carbon shift (Loutit and Kennett, 1979) from ~7 Ma to ~4 Ma. This shift is representative of what Loutit and Kennett (1979) describe as, “a permanent and important change in the paleoceanographic and geochemical state of the oceans,” indicative of a change in global abyssal circulation. This shift is represented by a 1.5 ± 0.25‰ drop in $\delta^{13}C$ values in both the planktonic and benthic records from Site 982.

Cross-plot

Data points from the benthic foraminiferal species *C. mundulus* and *P. wuellerstorfi* (**Fig. 12**, blue and purple, respectively) clustered mainly in the bottom middle region of the cross-plot. Relative to surface waters, deep waters are less affected by isotopic changes that result from glacial-interglacial cycles and annual temperature variability; as such, the isotope ratios of the tests of benthic foraminifera are less variable than those of the tests of planktonic foraminifera. Tests of benthic foraminifera often produce higher $\delta^{18}O$ values than their planktonic counterparts, as deepwater is colder than water in the upper water column and have higher $\delta^{18}O$ values. Additionally, the tests of benthic species tend to produce relatively low $\delta^{13}C$ values due to remineralization of isotopically light organic material in deepwater (Kroopnick, 1985); thus, benthic data points plot lower on the x-axis ($\delta^{13}C$) than most of the planktonic data points.

Data from the planktonic species *O. universa* and *G. bulloides* (**Fig. 12**, red and orange, respectively) plotted mainly in the upper region of the cross-plot. Tests of planktonic foraminifera often record lower $\delta^{18}O$ values than their benthic counterparts, reflecting the vertical temperature gradient; thus, planktonic data points mainly plot on the upper half of the y-axis ($\delta^{18}O$). Unlike the $\delta^{13}C$ values from the two benthic species, the $\delta^{13}C$ values from the two planktonic species greatly differ from one another. $\delta^{13}C$

values of *O. universa* cluster in a way similar to the clustered benthic data, but with much greater $\delta^{13}C$ values than those of the benthic foraminifera. *O. universa* tests produce particularly high $\delta^{13}C$ values because the zooxanthellae of the species preferentially sequester light ^{12}C during photosynthesis (Spero and DeNiro, 1987). As such, *O. universa* are left with more heavy carbon isotopes to incorporate into their tests (Spero and DeNiro, 1987).

G. bulloides is an asymbiotic species (Hemleben et al., 1988), so zooxanthellae do not affect the $\delta^{13}C$ values of *G. bulloides* tests, resulting in isotopically lighter tests than those of *O. universa*. As discussed in **Impact of vital effects on planktonic stable isotope values**, $\delta^{13}C$ and $\delta^{18}O$ values from *G. bulloides* are likely so variable due to vital effects related to the scale and seasonal nature of *G. bulloides* blooms and the fact that *G. bulloides* in the North Atlantic typically resides in the surface mixed layer (Fairbanks et al., 1982).

DISCUSSION

Comparison to biomarker proxies

A biomarker ($U^{k'}_{37}$) temperature proxy from North Atlantic carbonate samples was previously employed to reconstruct SSTs at Site 982 throughout the Miocene (Herbert et al., 2016). A side-by-side comparison of my temperature reconstructions and the $U^{k'}_{37}$ from Herbert et al. (2016) revealed that the absolute temperature estimates differ greatly, though the temperature trends indicated by both proxies are similar (**Fig. 13**). Herbert (2003) explains that alkenone temperature records may differ slightly from $\delta^{18}O$ temperature records as the result of a handful of phenomena: Alkenone-producing coccolithophores live most or all of their life in the shallow photic zone, where the water temperatures is the warmest, whereas planktonic foraminifera tend to live all or part of their lives in slightly deeper (thus colder) parts of the water column (e.g., the surface mixed layer or the thermocline, Wolfteich, 1994; Herbert, 2003). As such, water temperatures calculated from $\delta^{18}O$ from planktonic foraminifera report, on average, cooler water temperatures than those suggested by alkenone records (Herbert, 2003). This apparent cooling effect can be seen in **Fig. 13**. As $\delta^{18}O$ temperature records from planktonic foraminifera also account for changes in global ice volume, these temperature records may also be more variable in comparison to alkenone records (Herbert, 2003).

For this comparison, the age values associated with the $U^{k'}_{37}$ data from Herbert et al. (2016) were converted from core depth values from Herbert et al. (2016) using the age model created for this study (**Fig. 7**). The Middle and Late Miocene cooling trends described in the RESULTS corroborate the $U^{k'}_{37}$ data from Herbert et al. (2016). Similarly, the warming during the latest Late Miocene and earliest Early Pliocene can be seen in the $U^{k'}_{37}$ record, as well (Herbert et al., 2016). The large (~10°C) disparities between the $\delta^{18}O$ and $U^{k'}_{37}$ temperature estimates from ~7 to ~3 Ma do call into question which proxy produces more accurate temperature record reconstructions. Examining a different biomarker proxy (TEX_{86}) in the samples from Site 982 may shed some light on this issue.

Comparison to other sites in the WNAT

Of the other records from other sites in the WNAT, the records from Site 608 (42.84°N; Benaroya et al., 2018) correlate best with those from Site 982 (57.52°N; **Fig. 14**). The surface and benthic foraminiferal $\delta^{18}O$ records from Site 608 (from

Dentoglobigerina altispira and *Cibicidoides* spp. tests, respectively) both indicate a cooling trend from the late Middle Miocene through the latest Late Miocene, with more rapid cooling beginning between 9 Ma and 8 Ma (Benaroya et al., 2018). The data from Sites 563 (33.64°N; Bellino et al., 2018) and 558 (37.77°N; Galochkina et al., 2017; 2018) are difficult to correlate with data from Site 982, as the records only extend to about halfway through the timeframe of this study. To compound this issue, a portion of the data from Sites 563, 558, and 608 is not possible to correlate with the data from Site 982, as the latter site lacks isotope data between ~10.25 Ma to ~8.91 Ma (Bellino et al., 2018; Benaroya et al., 2018; Galochkina et al., 2017; 2018; Jansen et al., 1996). One expected trend that can be confirmed by $\delta^{18}O$ values from all four sites in the WNAT is that the average surface and deep-water temperatures increase moving southward along the WNAT (Bellino et al., 2018; Benaroya et al., 2018; Galochkina et al., 2017; 2018).

Conclusions and future work

Stable isotope ratios are indeed reliable proxies for reconstructing temperature records, and the trends these records reveal can be well-correlated to trends computed using biomarker proxies such as those used by Herbert et al. (2016). Specific water temperature measurements, however, differ significantly across these two types of proxies (**Fig. 13**). A larger number of data points from Site 982 would likely have made correlations among sites in the WNAT easier to recognize. More samples from the interval focused on in this study are slated to be analyzed in the coming months. Additionally, ongoing work by Keating et al. (2019) will expand the stable isotope record for Site 982 deeper into the Miocene, with the goal of documenting the effects of climatic events like the MMCT and MCO. This older portion of the Miocene record will overlap more with the age ranges in Bellino et al. (2018), Benaroya et al. (2018), and Galochkina et al. (2017; 2018); thus Keating et al. (2019) will allow for a more meaningful correlation of records across the WNAT. Keating et al. (2019) will also endeavor to correlate stable isotope records with biomarker proxy data from Site 982. Additionally, examining TEX_{86} records from Site 982 may shed some light on the disparities between the $\delta^{18}O$ and $U^{k'}_{37}$ temperature record reconstructions for this site.

REFERENCES CITED

Abelson, M. and Erez, J. (2017). The onset of modern-like Atlantic meridional overturning circulation at the Eocene-Oligocene transition: Evidence, causes, and possible implications for global cooling, *Geochemistry, Geophysics, Geosystems*, 18 (6), pp. 2177-2199.

Andersson, C. and Jansen, E. (2003). A Miocene (8-12 Ma) intermediate water benthic stable isotope record from the northeastern Atlantic, ODP Site 982, *Paleoceanography and Paleoclimatology*, 18 (1).

Baldauf, J.G., Thomas, E., Clement, B., Takayama, T., Weaver, P.P.E., Backman, J., Jenkins, G. Mudie, P.J., Westberg-Smith, M.J. (1987). *Magnetostratigraphic and biostratigraphic synthesis, Deep Sea Drilling Project Leg 94*, Shipboard Scientific Party, Deep Sea Drilling Project Site 608, pp. 1159-1205.

Bellino, L., Miller, K.G., Makarova, M., Rosenthal, Y., Zhou, X., Browning, J.V., Fircha, J., and Wright, J.D. (2018). North Atlantic Ocean sea surface temperatures during the Middle to Late Miocene, 18-8 million years ago, Geological Society America Annual Meeting, 2018.

Bemis, B.E., Spero, H.J., Lea, D.W., and Bijma, J. (2000). Temperature influence on the carbon isotopic composition of *Globigerina bulloides* and *Orbulina universa* (planktonic foraminifera), *Marine Micropaleontology*, 38 (3-4), pp. 213-228.

Benaroya, S., Miller, K.G., Makarova, M., Browning, J.V., and Wright, J.D. (2018). Miocene planktonic foraminiferal stable isotopes and sea surface temperatures at North Atlantic Site 608: Geological Society America Annual Meeting, 2018.

Bijma, J., Spero, H.J., and Lea, D.W. (1999). Reassessing foraminiferal stable isotope geochemistry: Impact of the oceanic carbonate system (experimental results), in *Use of Proxies in Paleoceanography*, Fischer, G. and Wefer, G. (eds.), pp. 489-512.

Boyle, P.R., Romans, B.W., Tucholke, B.E., Norris, R.D., Swift, S.A., and Sexton, P.F. (2017). Cenozoic North Atlantic deep circulation history recorded in contourite drifts, offshore Newfoundland, Canada, *Marine Geology*, 385, pp. 185-203.

Cramer, B.S., Miller, K.G., Barrett, P.J., and Wright, J.D. (2011). Late Cretaceous-Neogene trends in deep ocean temperature and continental ice volume: Reconciling records of benthic foraminiferal geochemistry ($\delta^{18}O$ and Mg/Ca) with sea level history, *Journal of Geophysical Research: Oceans*, 116 (C12023).

Fairbanks, R.G., Sverdlove, M., Free, R., Wiebe, P.H., and Bé, A.W.H. (1982). Vertical distribution and isotopic fractionation of living planktonic foraminifera from the Panama Basin, Nature, 298, pp. 841-844.

Galochkina, M., Miller, K.G., Makarova, M., Browning, J.V., and Wright, J.D. (2017). North Atlantic sea surface and thermocline temperature variations during the Middle-Late Miocene (16-8 Ma), Geological Society of America Annual Meeting, 2017.

Galochkina, M., Miller, K.G., Makarova, M., Browning, J.V., and Wright, J.D. (2018). Miocene North Atlantic sea surface and thermocline temperature variations (20-8 Ma), American Geophysical Union Fall Meeting, 2018.

Gradstein, F.M., Ogg, J.G., Schmitz, M.D., and Ogg, G.M. (2012). *The Geologic Time Scale*, Elsevier B.V., New York, NY. Print.

Hemleben, C., Spindler, M., and Anderson, O.R. (1988). *Modern Planktonic Foraminifera*, Springer-Verlag, New York, p. 10.

Herbert, T.D. (2003). Alkenone paleotemperature determinations, in *Treatise on Geochemistry*, Holland, H.D. and Turekian, K.K. (eds.), 6, pp. 391-432.

Herbert, T.D., Lawrence, K.T., Tzanova, A., Cleaveland Peterson, L., Caballero-Gill, R., and Kelly, C.S. (2016). Late Miocene global cooling and the rise of modern ecosystems, *Nature Geoscience*, 9, pp. 843-847.

Hohbein, M.W., Sexton, P.F., and Cartwright, J.A. (2012). Onset of North Atlantic Deep Water production coincident with inception of the Cenozoic global cooling trend, *Geology*, 40 (3), pp. 255-258.

Holbourn, A., Henderson, A.S., and MacLeod, N. (2013). *Atlas of Benthic Foraminifera*, Wiley-Blackwell, Oxford, UK. Print.

Jansen, E., Raymo, M.E., and Blum, P. (1996). *Proceedings of the Ocean Drilling Program, Initial Reports*, Shipboard Scientific Party, Ocean Drilling Program Site 982, pp. 91-138.

Keating, R., Makarova, M., McLellan, O., Miller, K.G., Mortlock, R.A., Wright, J.D. Thermal evolution of the northern North Atlantic during the Early-Middle Miocene from ODP Site 982 record, Abstract PP21B-1613 presented at 2019 Fall Meeting, AGU, San Francisco, CA, 9-13 Dec.

Kennett, J.P. and Srinivasan, M.S. (1983). *Neogene Planktonic Foraminifera: A Phylogenetic Atlas*, Hutchinson Ross, New York, NY. Print.

Kim, S. and O'Neil, J.R. (1997). Equilibrium and nonequilibrium oxygen isotope effects in synthetic carbonates, *Geochimica et Cosmochimica Acta*, 61 (16) pp. 3461-3475.

Kroopnick, P. M. (1985), The distribution of ^{13}C of ΣCO_2 in the world oceans, *Deep Sea Research Part A. Oceanographic Research Papers*, 32-1, pp. 57-84.

Lawrence, K.T., Herbert, T.D., Brown, C.M., Raymo, M.E., and Haywood, A.M. (2009). High-amplitude variations in North Atlantic sea surface temperature during the Early Pliocene warm period, *Paleoceanography*, 24, PA2218.

Loutit, T.S. and Kennet, J.P. (1979). Application of carbon isotope stratigraphy to Late Miocene shallow marine sediments, New Zealand, Science, 204 (4398), pp. 1196-1199.

Makarova, M., Galochkina, M., Benaroya, S., Bellino, L., Fircha, J., Miller, K.G., Rosenthal, Y., Browning, J.V., and Wright, J.D. (2018). Evolution of Atlantic Meridional Overturning Circulation and meridional thermal gradients during the Miocene from legacy DSDP and ODP sites, American Geophysical Union Annual Meeting, 2018.

Miller, K.G., Feigenson, M.D., Wright, J.D., and Clement, B. (1991). Miocene isotope reference section, Deep Sea Drilling Project Site 608: An evaluation of isotope and biostratigraphic resolution, *Paleoceanograph*y, 6, pp. 33-52.

Miller, K.G., and Katz, M.E. (1987). Oligocene to Miocene benthic foraminiferal and abyssal circulation changes in the North Atlantic, *Micropaleontology*, 33 (2), pp. 97-149.

Miller, K.G., Mountain, G.S., Browning, J.V., Kominz, M., Sugarman, P.J., Christie-Blick, N., Katz, M.E., and Wright, J.D. (1987). Cenozoic global sea level, sequences, and the New Jersey transect: Results from coastal plain and continental slope drilling, *Reviews of Geophysics*, 36 (4), pp. 569-601.

Miller, K.G., Wright, J.D., and Fairbanks, R.G. (1991). Unlocking the Ice House: Oligocene-Miocene oxygen isotopes, eustasy, and margin erosion, *Journal of Geophysical Research*, 6, pp. 6829-6848.

Morozov, E.G., Demidov, A.N., Tarakanov, R.Y., and Zenk, W. (2010). Deep water masses of the South and North Atlantic, *Abyssal Channels in the Atlantic Ocean Water Structure and Flows,* Springer, pp. 25-50.

Ocean Drilling Stratigraphic Network (2011). Converted Ages, GEOMAR, Research Center for Marine Geosciences/Kiel, and the Geological Institute of the University Bremen. Retrieved from: http://www.odsn.de/cgi-bin/conv_ts.pl.

Pagani, M., Arthur, M.A., and Freeman, K.H. (1999). Miocene evolution of atmospheric carbon dioxide, *Paleoceanography*, 14, pp. 273-292.

Poore, H.R., White, N., and Jones, S. (2009). A Neogene chronology of Iceland plume activity from V-shaped ridges, *Earth and Planetary Science Letters*, 283 (1-4), pp. 1-13.

Raymo, M.E., Hodell, D., and Jansen, E. (1992). Response of deep ocean circulation to initiation of Northern Hemisphere Glaciation 3-2 Ma, *Paleoceanography*, 7, pp. 645-672.

Raymo, M.E., Oppo, D.W., Flower, B.P., Hodell, D.A., McManus, J.F., Venz, K.A., Kleiven, K.F., and McIntyre, K. (2004). Stability of North Atlantic water masses in face of pronounced climate variability during the Pleistocene, *Paleoceanography*, 19, PA2008.

Reid, J.L. and Mantyla, A.W. (1994). World dataset, Retrieved from: https://www.pmel.noaa.gov/epic/ewb/ewb_aboutreid.htm.

Roberts, D.G. and Deacon, G.E.R. (1975). Marine geology of the Rockall Plateau and Trough, *Philosophical Transactions of the Royal Society of London. Series A, Mathematical and Physical Sciences*, 278. Print.

Ryan, W.B.F., Carbotte, S.M., Coplan, J.O., O'Hara, S., Melkonian, A., Arko, R., Weissel, R.A., Ferrini, V., Goodwillie, A., Nitsche, F., Bonczkowski, J., and Zemsky, R. (2009). Global Multi-Resolution Topography synthesis, *Geochemistry, Geophysics, Geosystems*, 10 (3).

Savin, S.M., Abel, L., Barrera, E., Hodell, D.A., Kennett, J.P., Murphy, M., Keller, G., Killingley, J., and Vincent, E. (1985). The evolution of Miocene surface and near-surface marine temperatures: Oxygen isotopic evidence, *Geological Society of America Memoirs*, 163, pp. 49-82.

Scher, H.D. and Martin, E.E. (2006). Timing and climatic consequences of the opening of Drake Passage, *Science*, 312 (5772), pp. 428-430.

Scher, H.D., Whittaker, J.M., Williams, S.E., Latimer, J.C., Kordesch, W.E.C., Delaney, M.L. (2015). Onset of Antarctic Circumpolar Current 30 million years ago as Tasmanian Gateway aligned with westerlies, *Nature*, 523, pp. 580-583.

Spero, H.J., Bijma, J., Lea, D.W., and Bemis, B.E. (1997). Effect of seawater carbonate concentration on foraminiferal carbon and oxygen isotopes, *Nature*, 390, pp. 497-500.

Spero, H.J. and DeNiro, M.J. (1987). The influence of symbiont photosynthesis on the $\delta^{18}O$ and $\delta^{13}C$ values of planktonic foraminiferal shell calcite, *Symbiosis*, 4, pp. 213-228.

Super, J.R., Thomas, E., Pagani, M., Huber, M., O'Brien, C., and Hull, P.M. (2018). North Atlantic temperature and pCO_2 coupling in the Early-Middle Miocene, *Geology*, 46 (6), pp. 519-522.

Thunell, R. and Belyea, P. (1982). Neogene planktonic foraminiferal biogeography of the Atlantic Ocean, *Micropaleontology*, 28 (4), pp. 381-398.

Wolfteich, C.M. (1994). Satellite-derived sea surface temperature, mesoscale variability, and foraminiferal production in the North Atlantic, unpublished.

Woodard, S.C, Rosenthal, Y., Miller, K.G., Wright, J.D., Chiu, B.K, and Lawrence, K.T (2014). Antarctic role in northern hemisphere glaciation, *Science*, 346 (6211), pp. 847-851.

Worthington, L.V. (1976). On the North Atlantic circulation, *Johns Hopkins Oceanographic Studies*, The Johns Hopkins University Press, 6. Print.

Wright, J.D., Miller, K.G., and Fairbanks, R.G. (1991). Evolution of deep water circulation: Evidence from the Late Miocene Southern Ocean, *Paleoceanography*, 6, pp. 275-290.

Wright, J.D., Miller, K.G., and Fairbanks, R.G. (1992). Early and Middle Miocene stable isotopes: Implications for deepwater circulation, climate and tectonics, *Paleoceanography*, 7, pp. 357-389.

Wright, J.D., and Miller, K.G. (1993). Southern Ocean influences on Late Eocene to Miocene deepwater circulation, *The Antarctic Paleoenvironment*, 60, pp. 1-25.

Wright, J.D., and Miller, K.G. (1996). Control of North Atlantic Deep Water circulation by the Greenland-Scotland Ridge, *Paleoceanography*, 11 (2), pp. 157-170.

Zachos, J., Pagani, M., Sloan, L., Thomas, E., and Billups, K. (2001). Trends, rhythms, and aberrations in global climate 65 Ma to present, *Science*, 292 (5517), pp. 686-693.

FIGURES

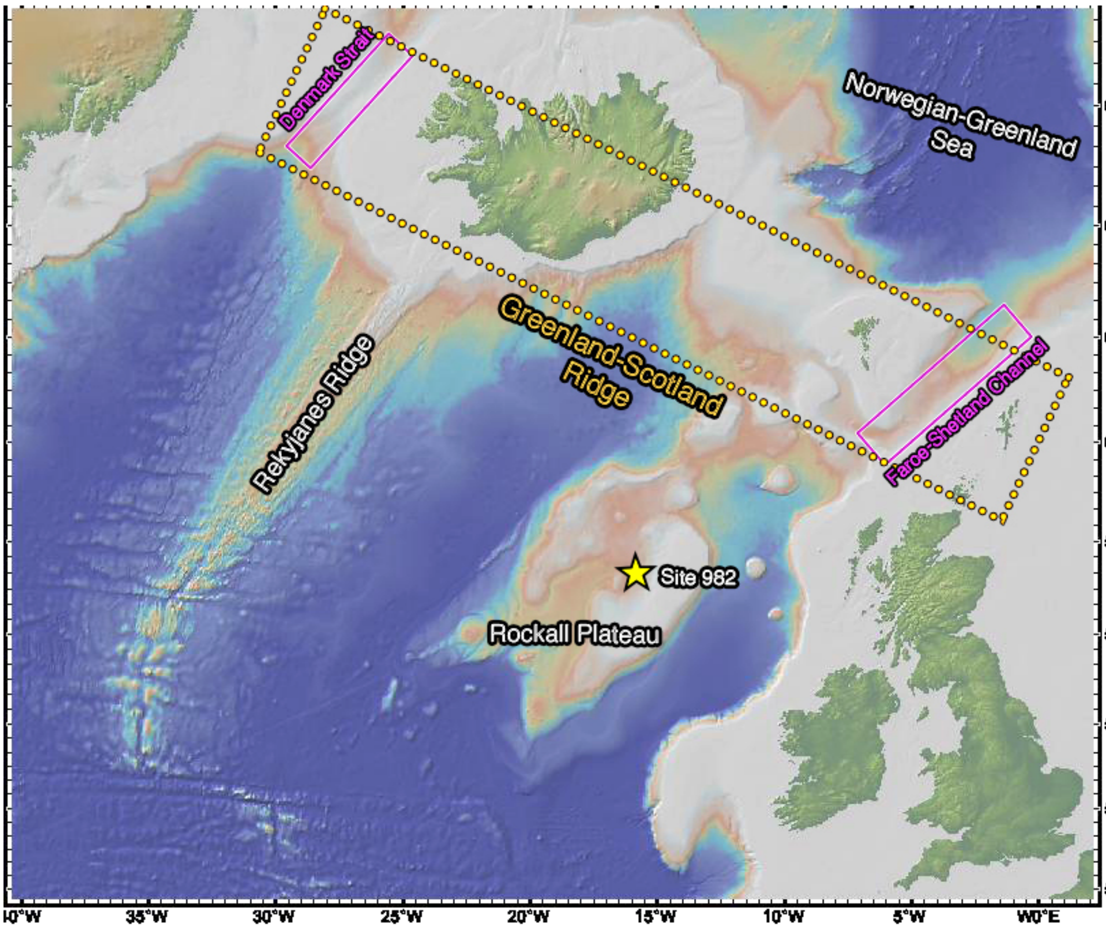

Figure 1. A map depicting Site 982 in relation to the Greenland-Scotland Ridge and environs. (Adapted from Poore et al., 2009; Ryan et al., 2009)

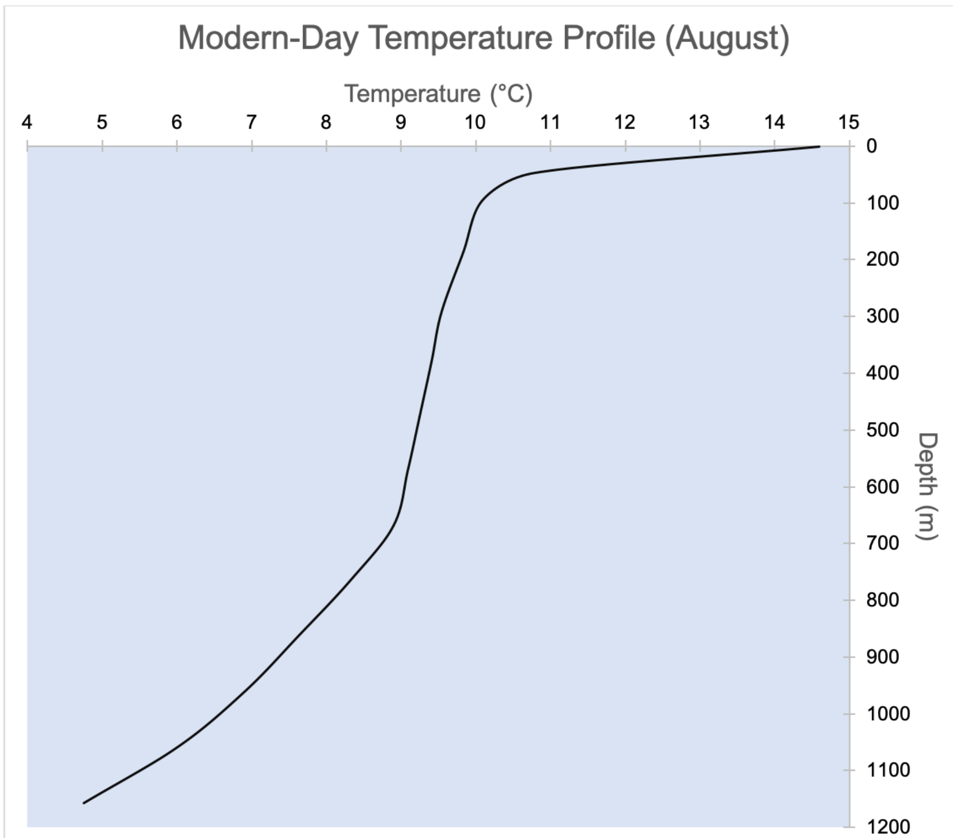

Figure 2. A near-modern August temperature profile of the water column above Rockall Plateau taken at 57.63°N, 16.35°W. (Adapted from Reid and Mantyla, 1994)

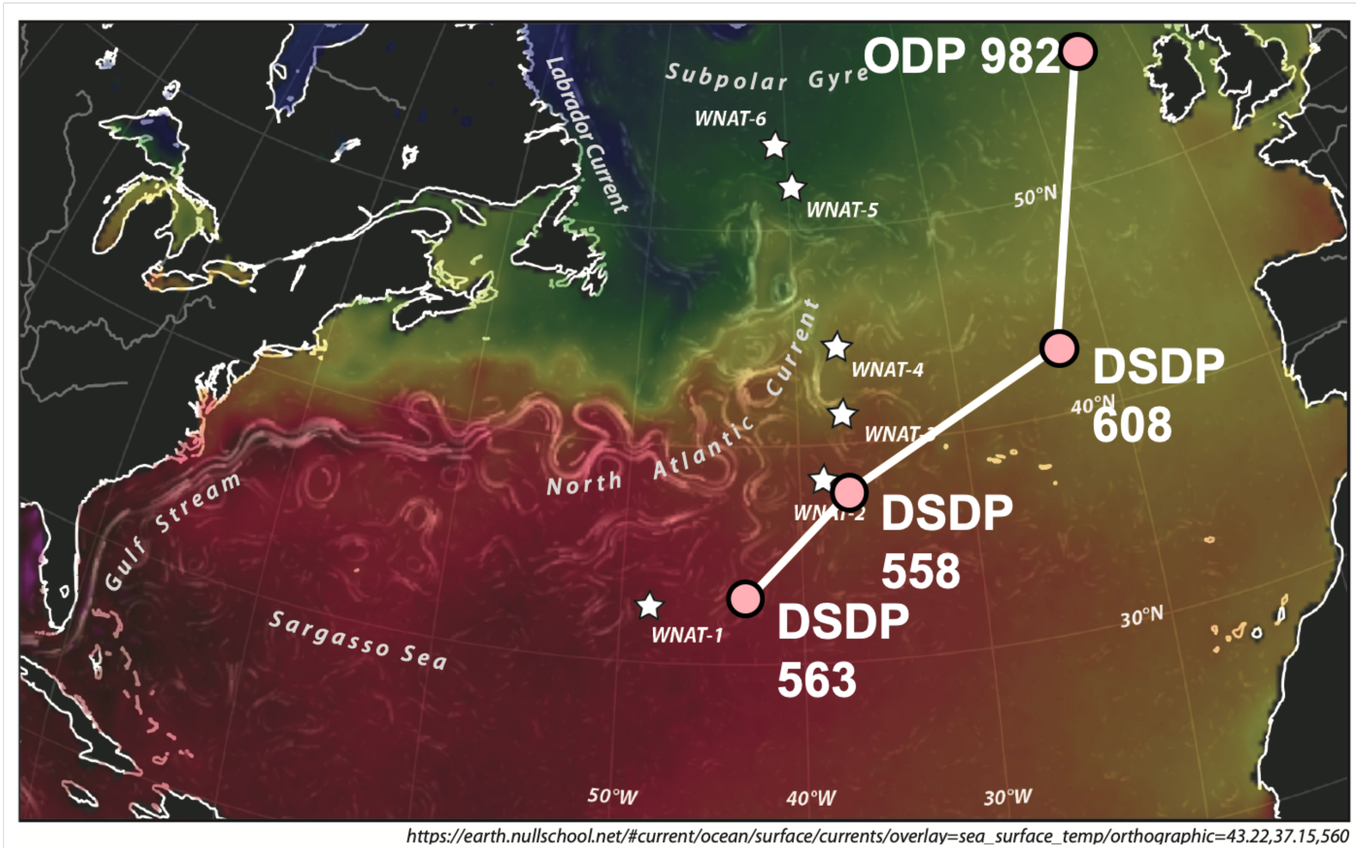

Figure 3. The Western North Atlantic Transect (WNAT), including Deep Sea Drilling Project (DSDP) Sites 563 (33.64°N), 558 (37.77°N), 608 (42.84°N), and Ocean Drilling Project (ODP) Site 982 (57.52°N).

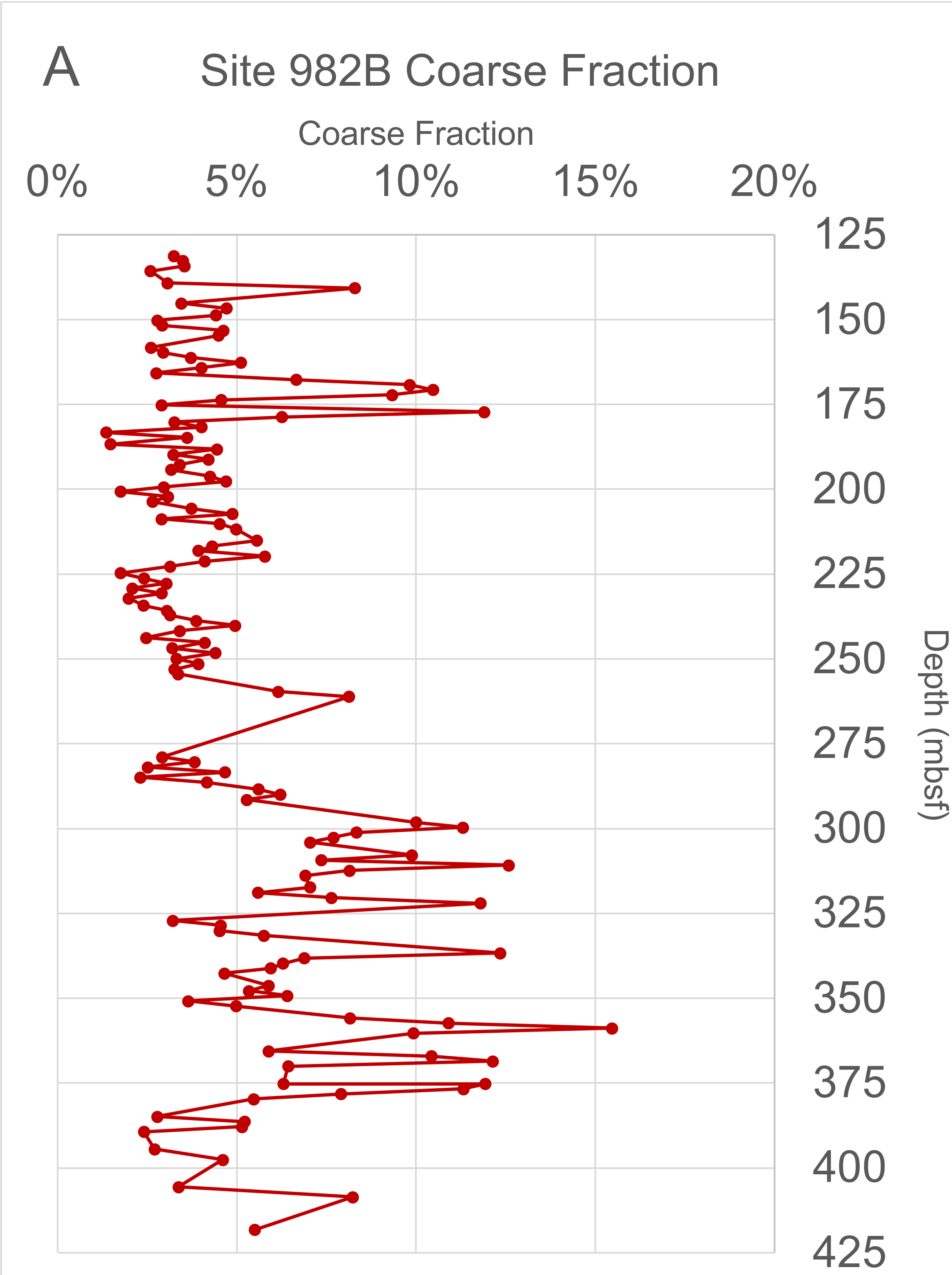

A
Site 982B Coarse Fraction
Coarse Fraction
0%
5%
10%
15%
20%
125
150
175
200
225
250
275
300
325
350
375
400
425
Depth (mbsf)

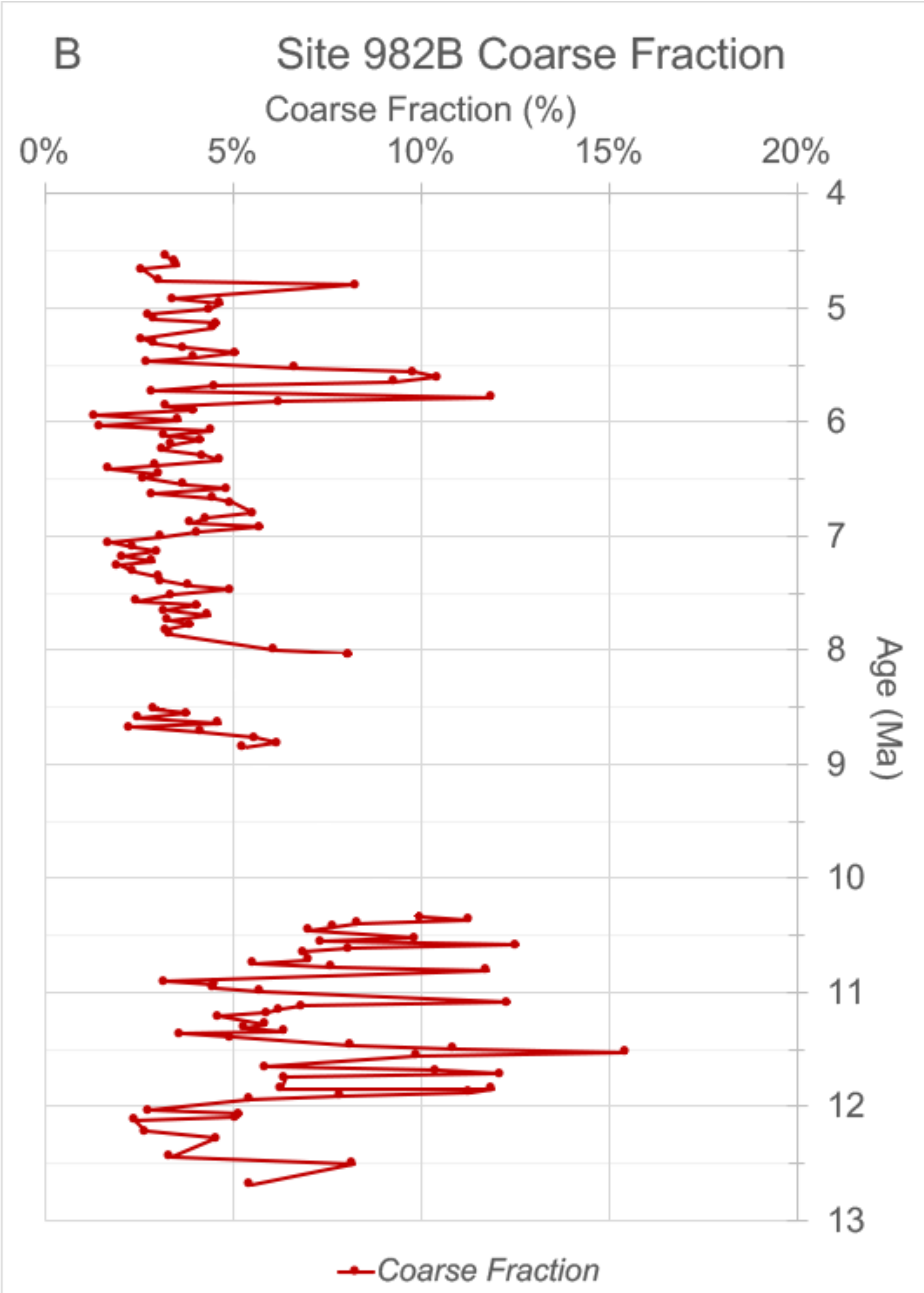

Figure 4. The coarse (>63 μm) fraction data (**Table 2**) from all 134 samples plotted against **A)** depth and **B)** age. Percent values are fractions of the original mass of each sample.

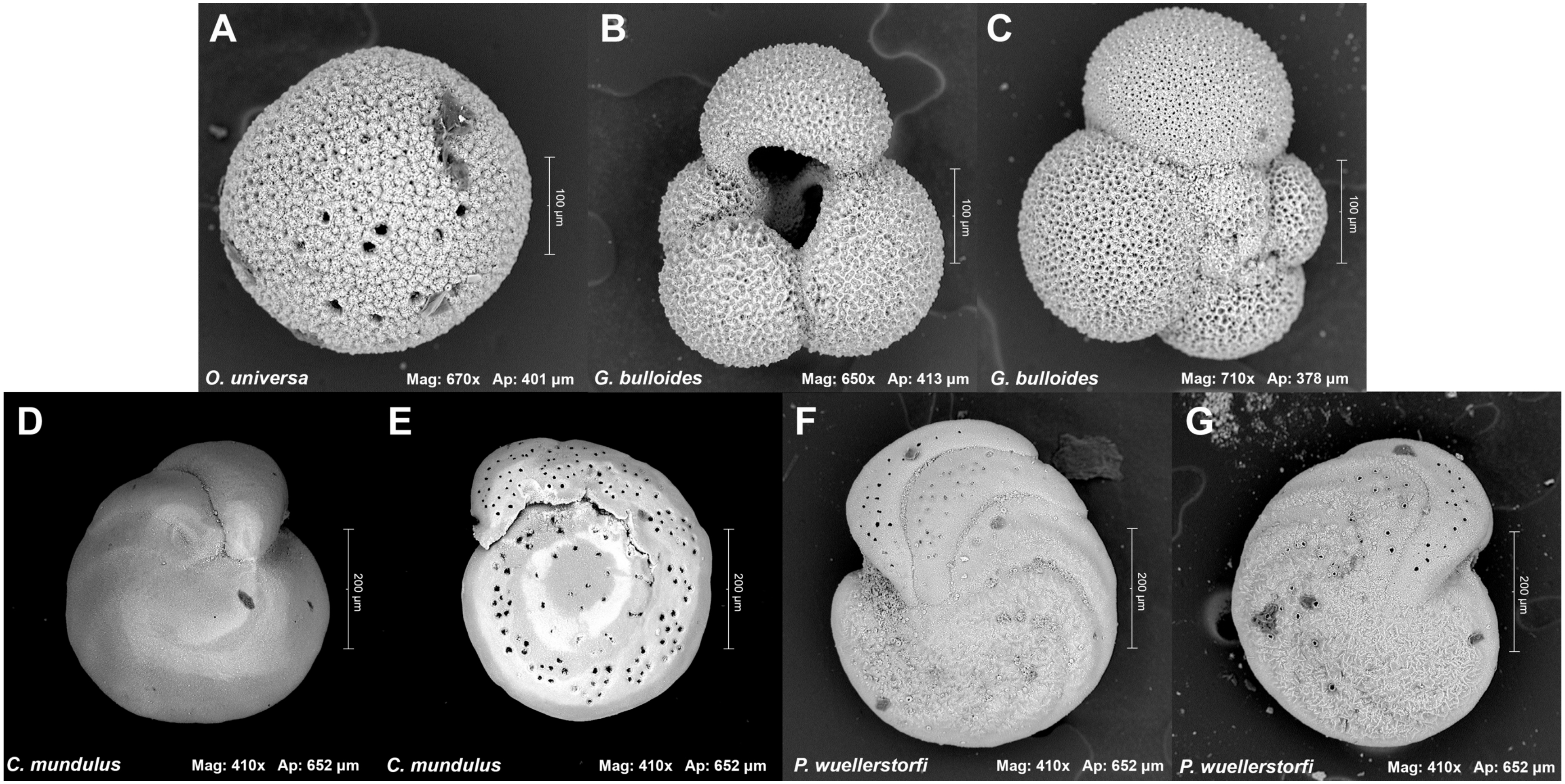

Figure 5. Scanning electron microscope images of individuals of the species used in this study. **A)** *Orbulina universa* **B-C)** *Globigerina bulloides* **D-E)** *Cibicidoides mundulus* **F-G)** *Planulina wuellerstorfi*

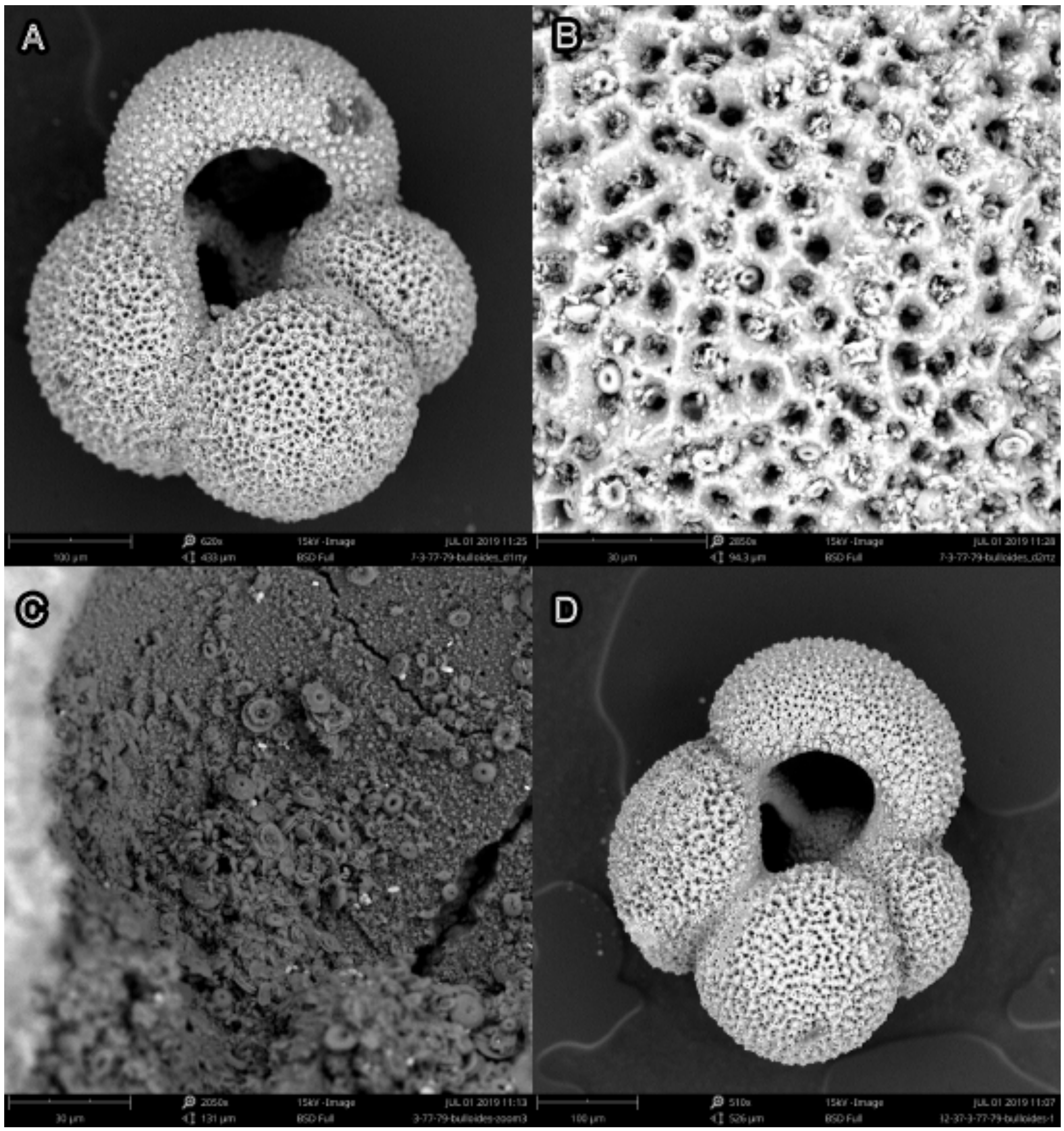

Figure 6. Scanning electron microscope images of **A)** a *Globigerina bulloides* (*G. bulloides*) test that has not been sonicated, **B)** nannofossils in the pores of a *G. bulloides* test that has not been sonicated, **C)** nannofossils on the inside of a *G. bulloides* test that has not been sonicated, and **D)** a *G. bulloides* test that has been sonicated. Note that not all of pores in **D** are devoid of nannofossils, but that the pores in **D** are clearer relative to those in **A** and **B**.

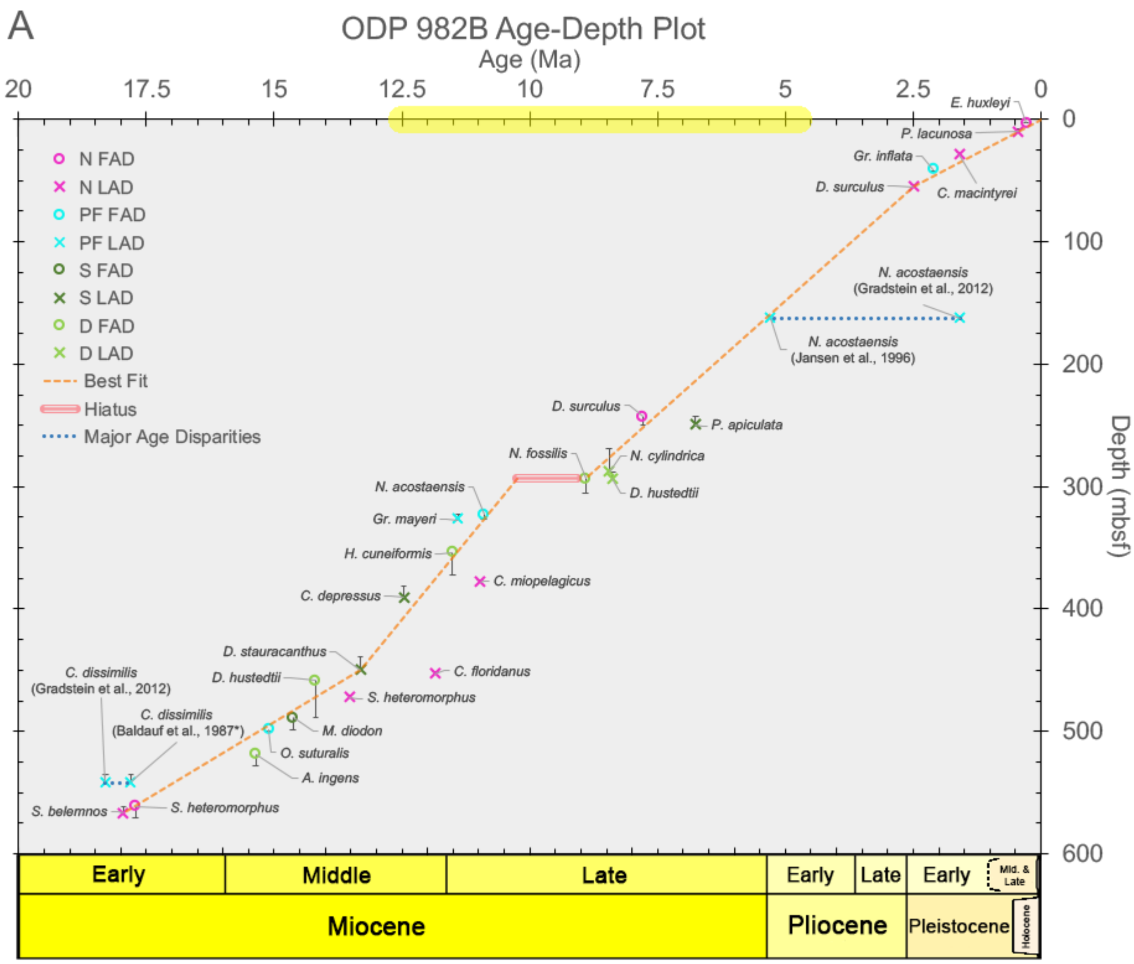
A
ODP 982B Age-Depth Plot
Age (Ma)
20
17.5
15
12.5
10
7.5
5
2.5
0
Depth (mbsf)
0
100
200
300
400
500
600
N FAD
N LAD
PF FAD
PF LAD
S FAD
S LAD
D FAD
D LAD
Best Fit
Hiatus
Major Age Disparities
E. huxleyi
P. lacunosa
Gr. inflata
D. surculus
C. macintyrei
N. acostaensis
(Gradstein et al., 2012)
N. acostaensis
(Jansen et al., 1996)
D. surculus
P. apiculata
N. fossilis
N. cylindrica
D. hustedtii
N. acostaensis
Gr. mayeri
H. cuneiformis
C. miopelagicus
C. depressus
D. stauracanthus
C. floridanus
C. dissimilis
(Gradstein et al., 2012)
D. hustedtii
S. heteromorphus
C. dissimilis
(Baldauf et al., 1987*)
M. diodon
O. suturalis
A. ingens
S. belemnos
S. heteromorphus
Early
Middle
Late
Early
Late
Early
Mid. & Late
Miocene
Pliocene
Pleistocene
Holocene

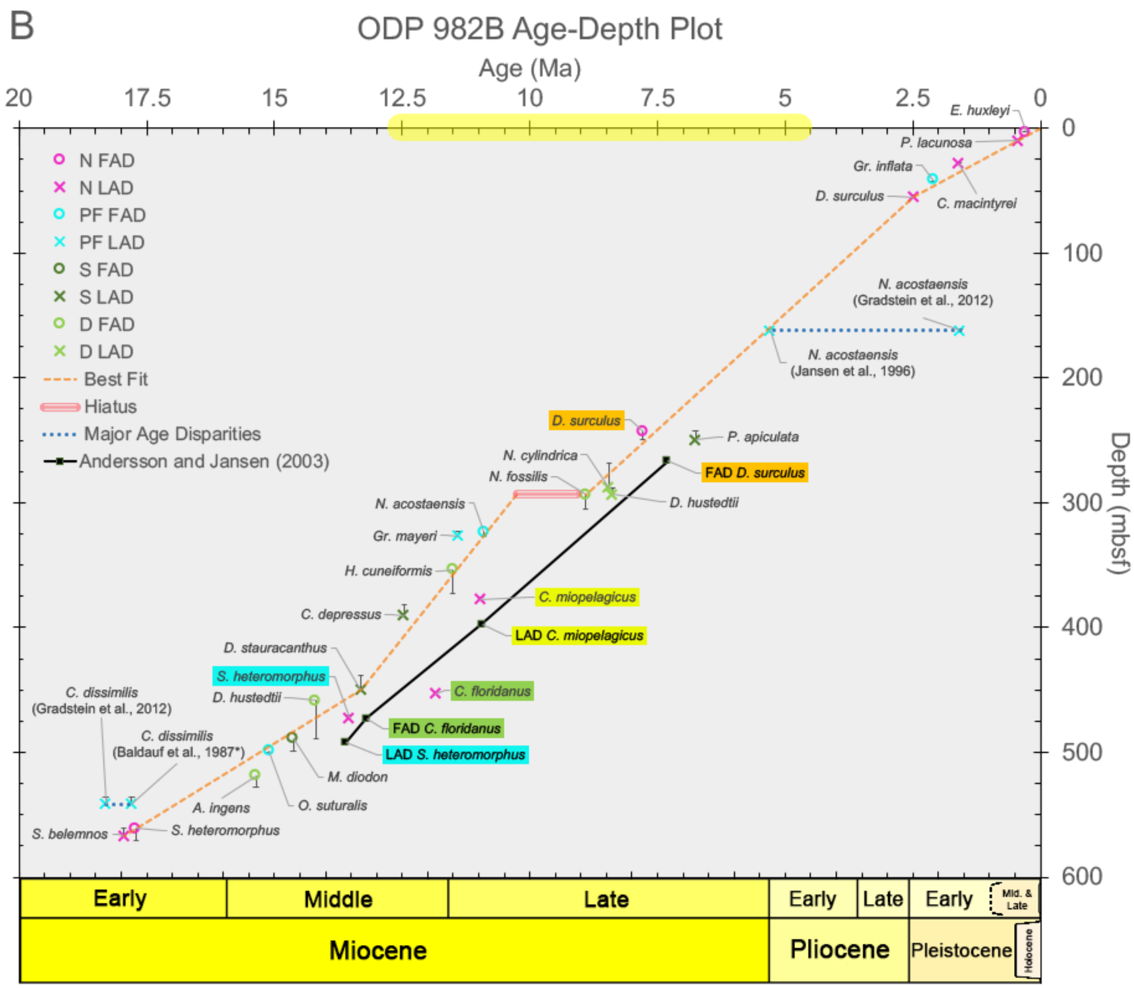

Figure 7. A) The age model created for this study (Jansen et al., 1996; ODSN, 2011; Gradstein et al., 2012). The highlighted portion of the x-axis marks the age range of samples used in this study. **B)** A comparison of the age model created for this study, and the age model used by Andersson and Jansen (2003) (black line). Highlighted FAD and LAD data show the differences in the first and last appearance data used in each study. The equations for each interval can be found in **Table 3**.

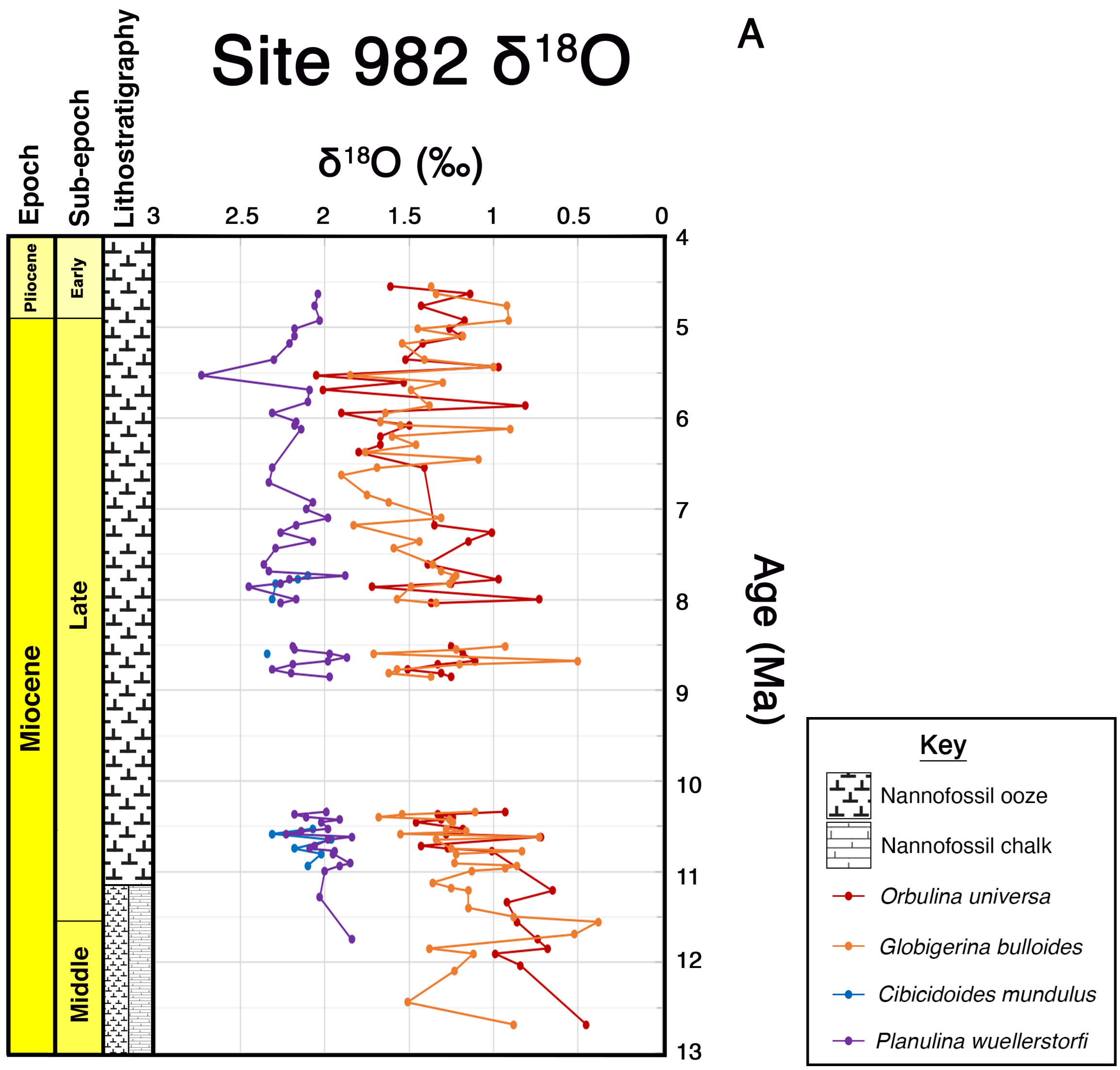
Site 982 δ18O
A
δ18O (‰)
3
2.5
2
1.5
1
0.5
0
Epoch
Sub-epoch
Lithostratigraphy
Pliocene
Miocene
Early
Late
Middle
Age (Ma)
4
5
6
7
8
9
10
11
12
13
Key
Nannofossil ooze
Nannofossil chalk
Orbulina universa
Globigerina bulloides
Cibicidoides mundulus
Planulina wuellerstorfi

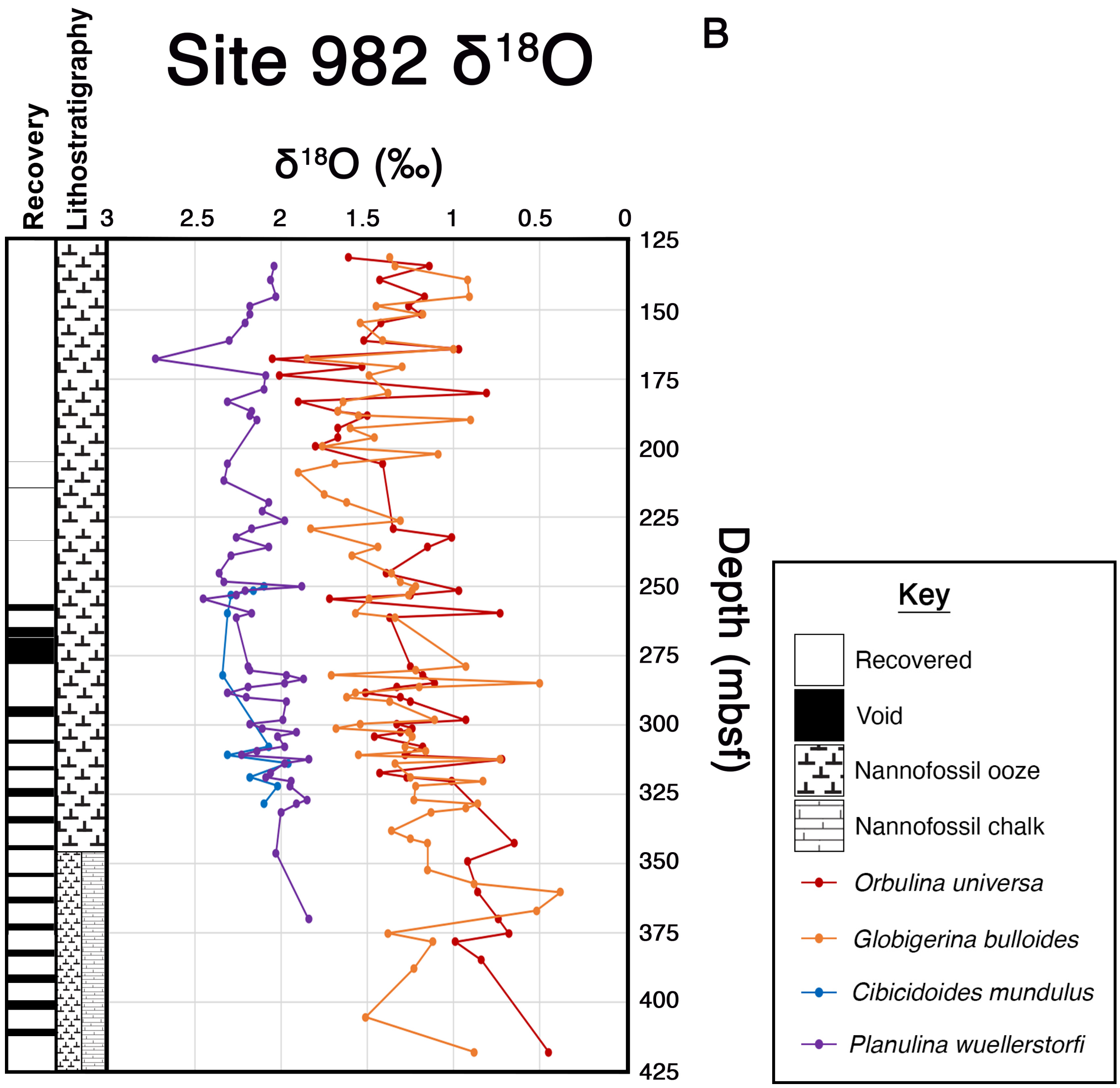

Figure 8. Stable oxygen isotope data (**Table 4**) from this study **A)** vs age and **B)** vs depth. These values decrease from the late Middle Miocene through the latest Late Miocene. The values briefly increase at the beginning of the earliest Early Pliocene, then decrease once again.

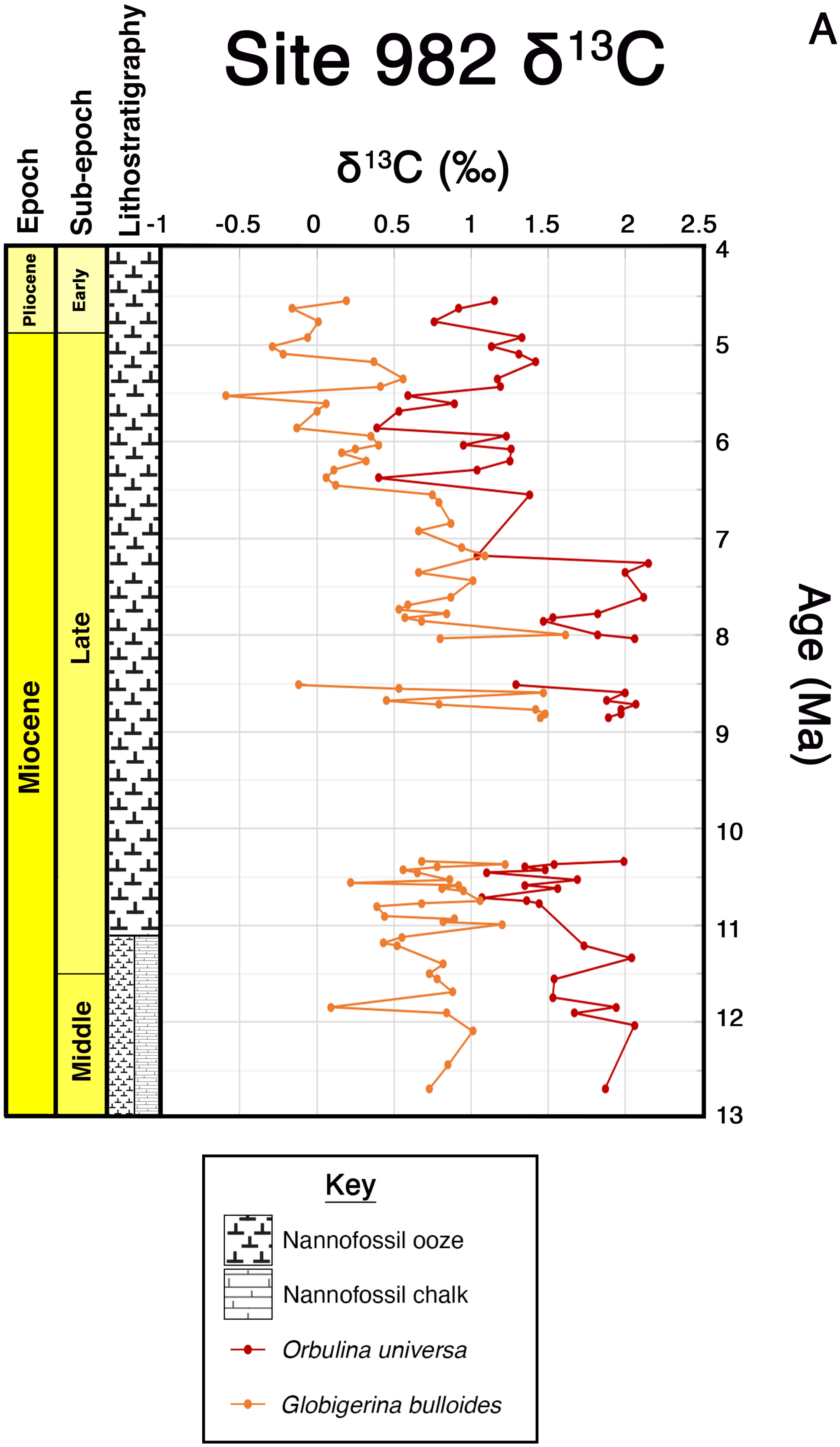
A
Site 982 δ13C
δ13C (‰)
Epoch
Sub-epoch
Lithostratigraphy
-1
-0.5
0
0.5
1
1.5
2
2.5
4
5
6
7
8
9
10
11
12
13
Age (Ma)
Pliocene
Miocene
Early
Late
Middle
Key
Nannofossil ooze
Nannofossil chalk
Orbulina universa
Globigerina bulloides

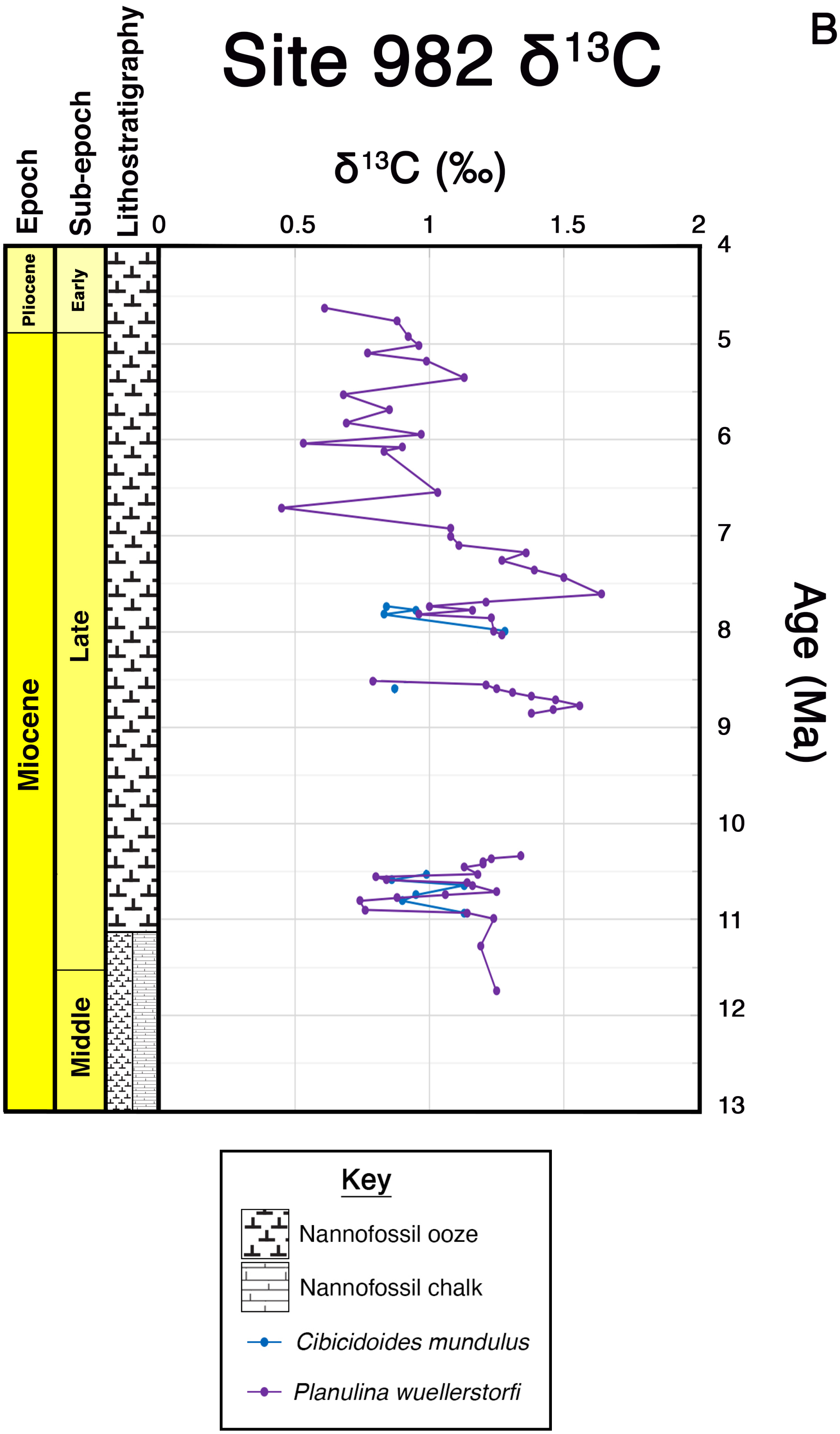
B
Site 982 δ13C
Epoch
Sub-epoch
Lithostratigraphy
δ13C (‰)
0
0.5
1
1.5
2
4
5
6
7
8
9
10
11
12
13
Age (Ma)
Pliocene
Early
Miocene
Late
Middle
Key
Nannofossil ooze
Nannofossil chalk
Cibicidoides mundulus
Planulina wuellerstorfi

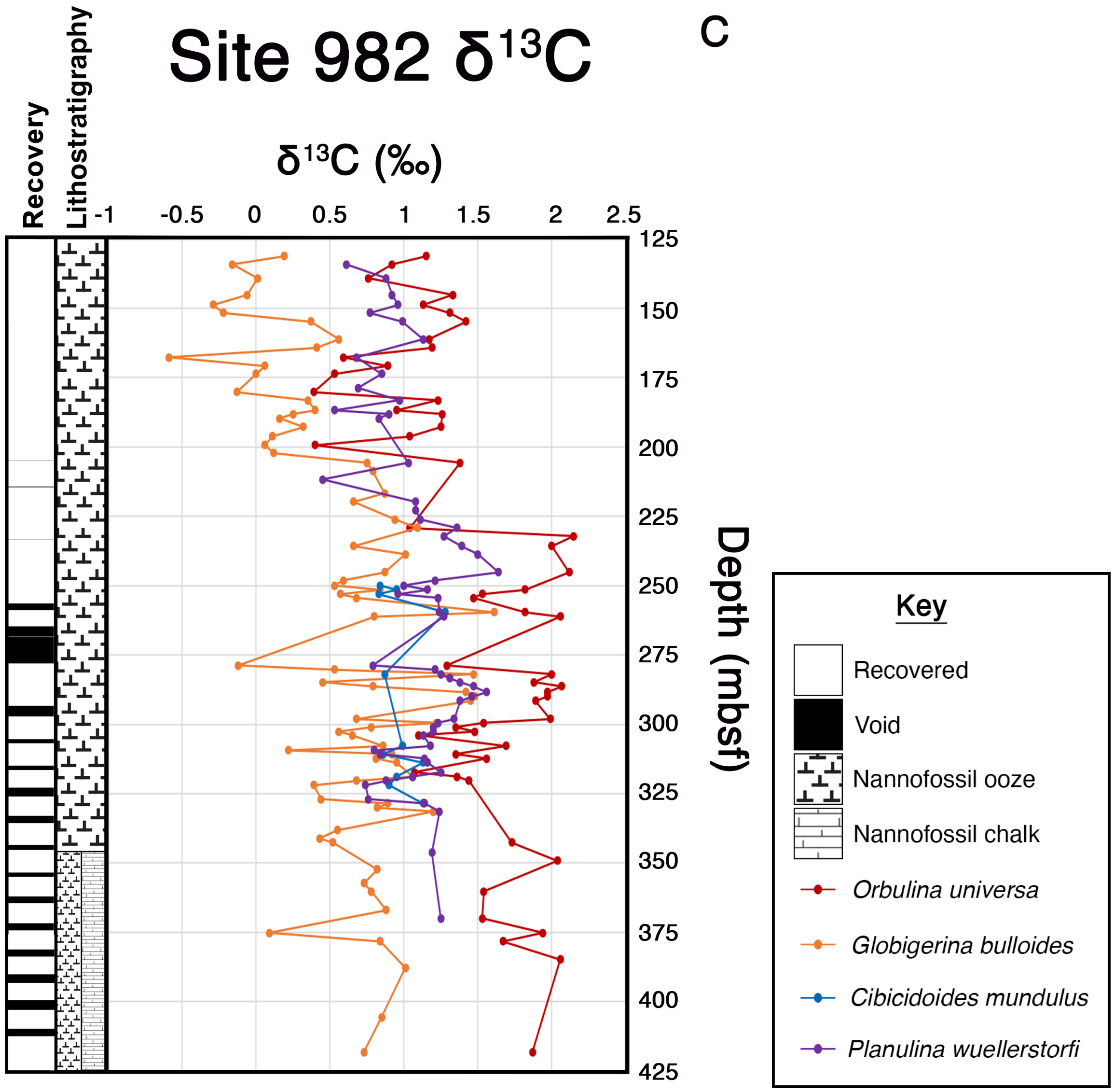

Figure 9. Stable carbon isotope data (**Table 4**) from this study. **A)** Isotope record from planktonic species. Note that the data from *G. bulloides* varies across a relatively large range of $\delta^{13}C$ values. This variability is likely due to the tendency of *G. bulloides* in the North Atlantic to bloom during peak springtime algal blooms (Wolfteich, 1994). **B)** Isotope record from benthic species. The data from these two species correspond very well, relative to the planktonic data. **C)** Data plotted against depth.

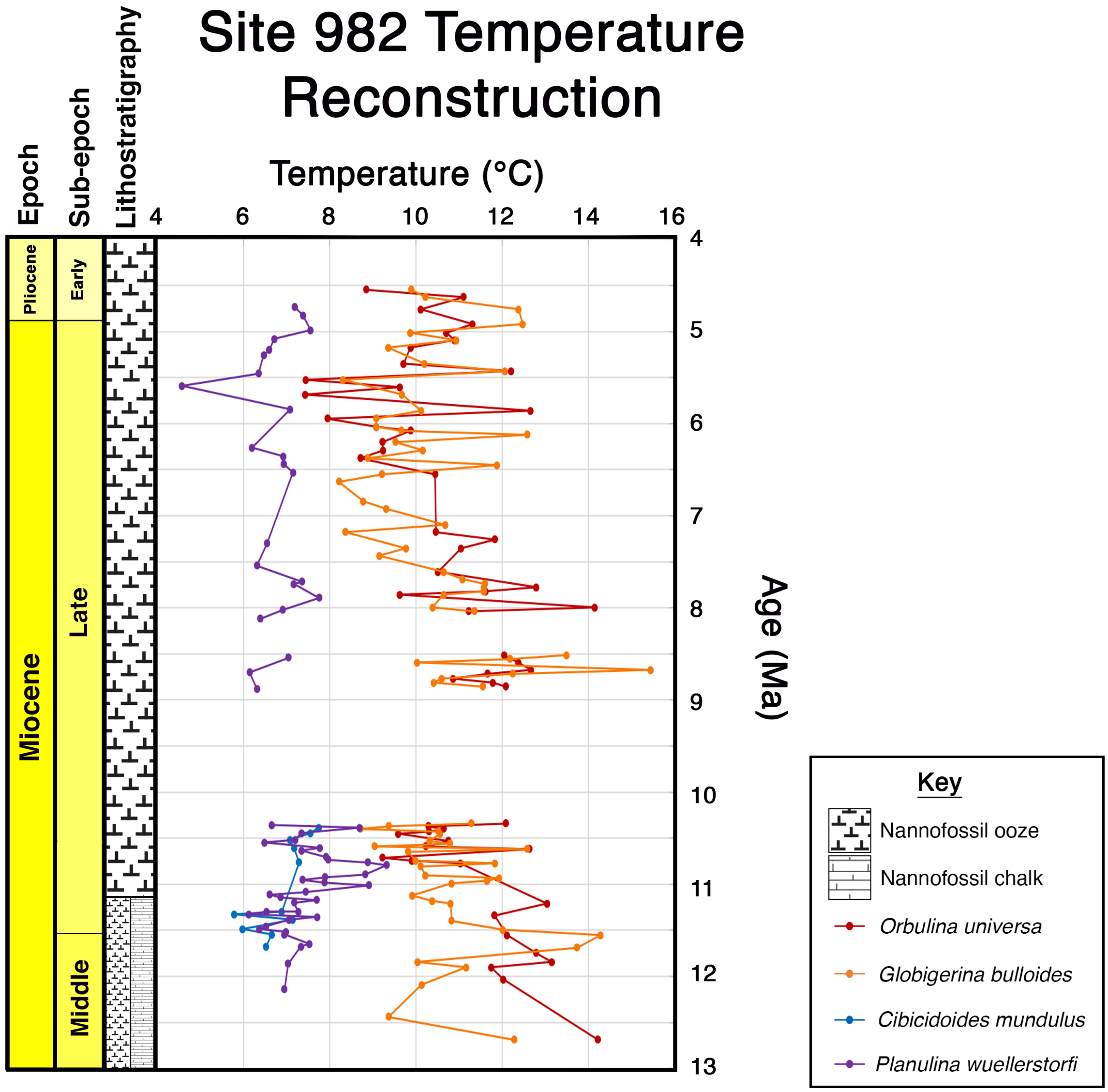

Figure 10. Water temperature values (**Table 5**) computed from $\delta^{18}O$ values (**Fig. 8**) and $\delta^{18}O_{seawater}$ after Cramer et al. (2011). Both planktonic and benthic species indicate a cooling trend throughout the majority of this timeframe. The magnitude of this cooling markedly increased in the latest Late Miocene. Temperatures began to rise again during the latest Late Miocene and into the earliest Early Pliocene, though the youngest samples indicate that temperatures began to drop again shortly after this rise.

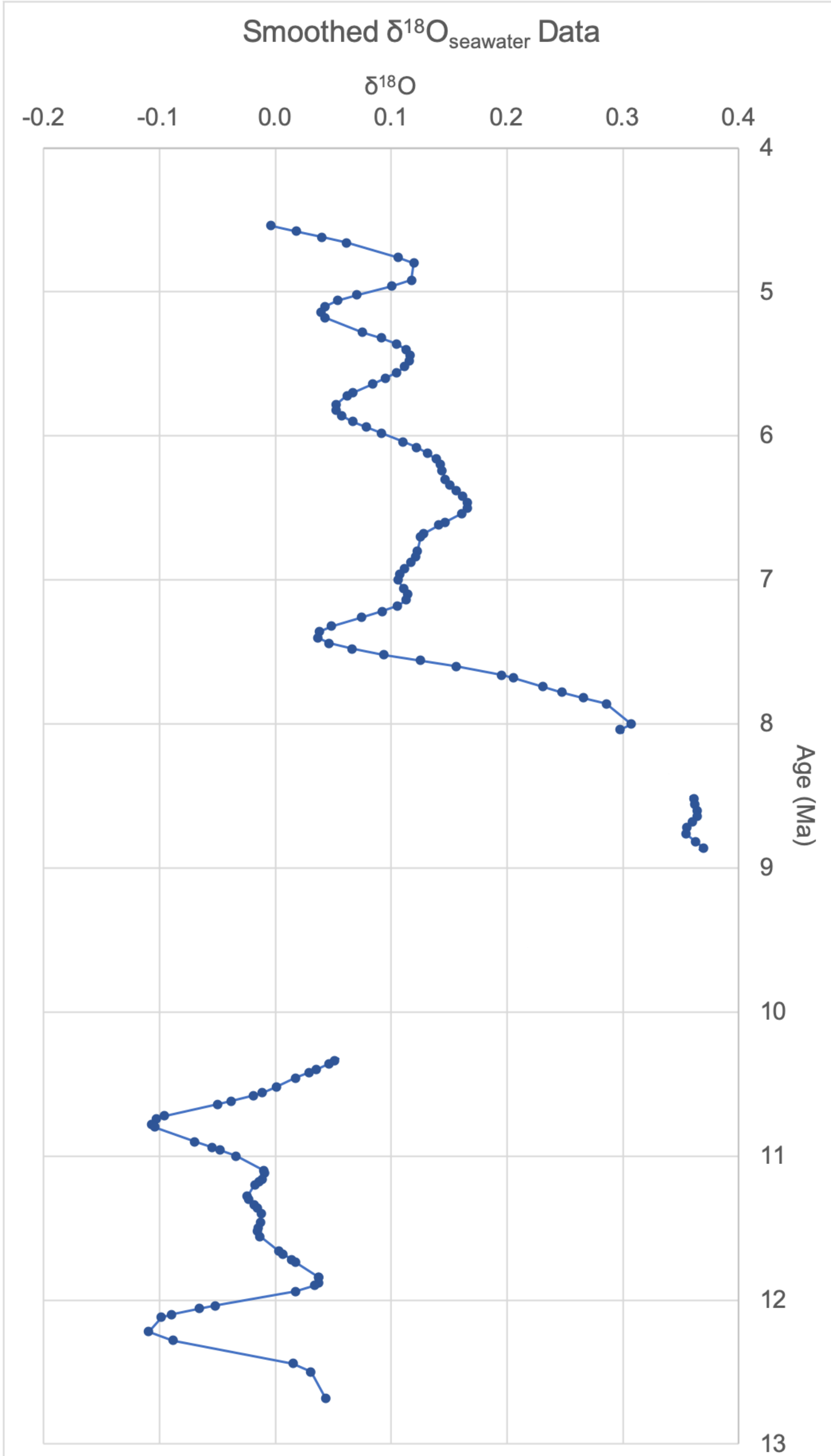

Figure 11. Smoothed $\delta^{18}O_{seawater}$ values from Cramer et al. (2011) used to calculate temperature values (**Fig. 10**).

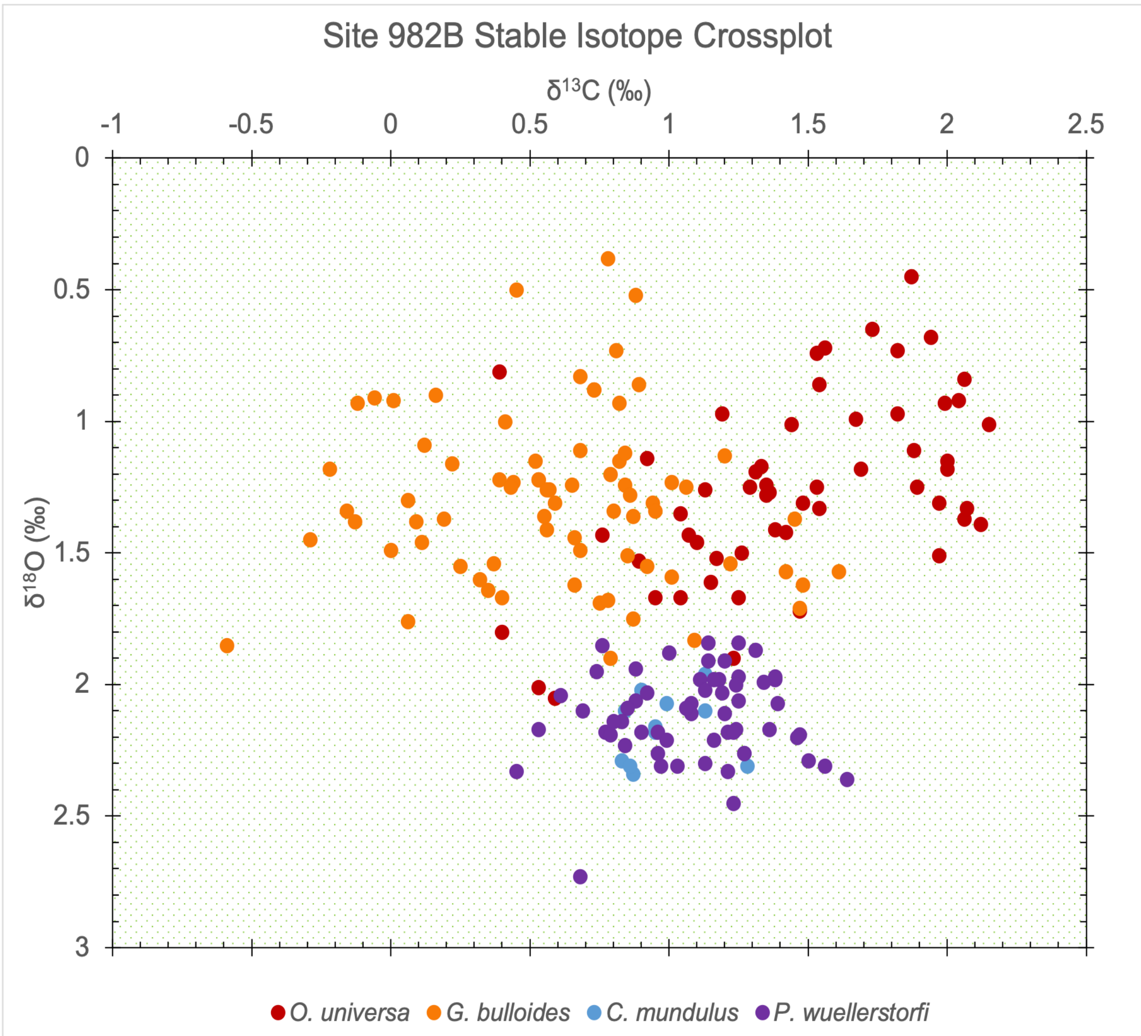

Figure 12. A cross-plot of the stable isotope data from this study.

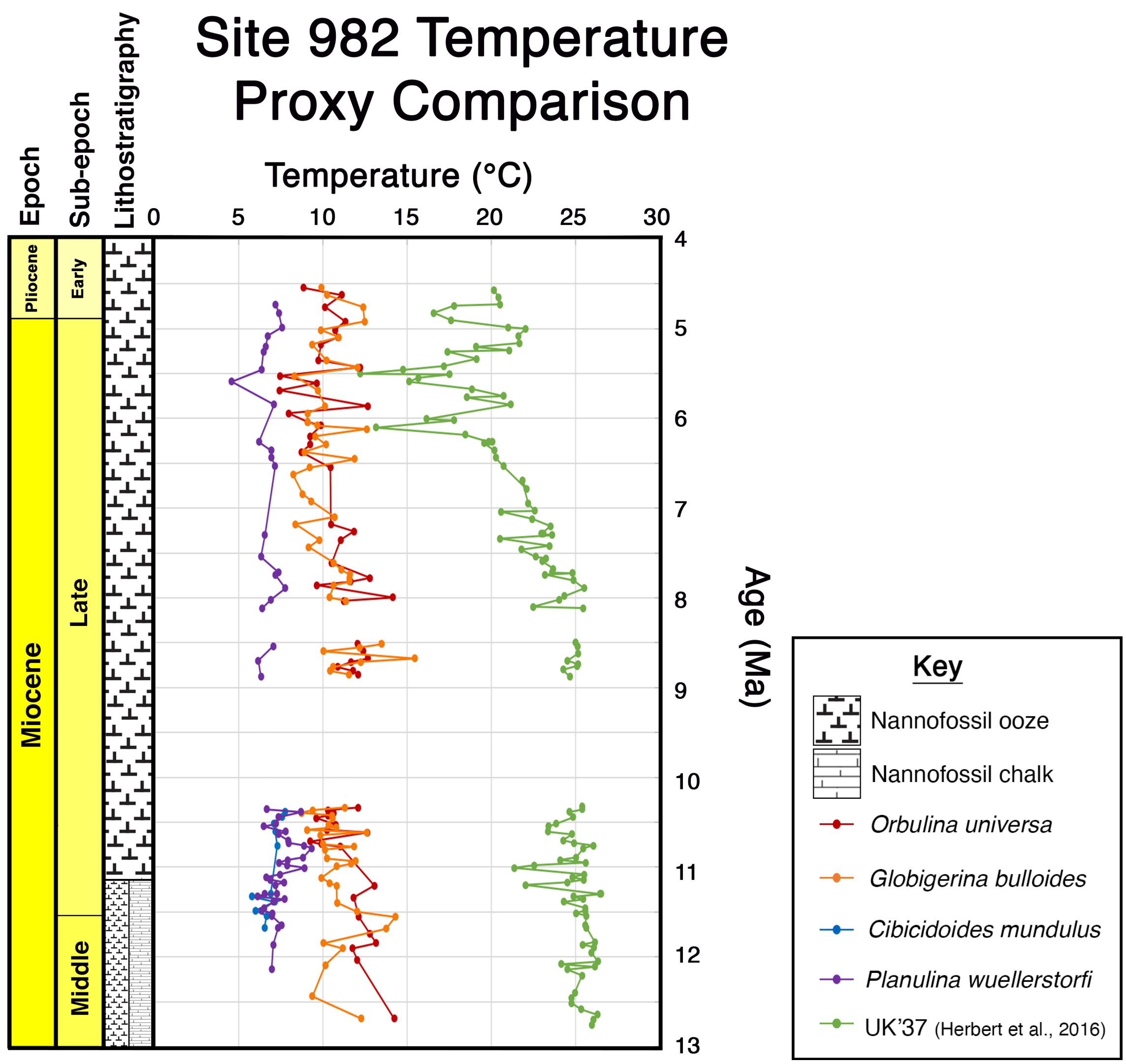

Figure 13. A comparison of the temperature data from this study (**Fig. 10**) and biomarker ($U^{k'}_{37}$) data temperature estimates from Herbert et al. (2016). Though the actual temperature estimates are quite different, similar temperature trends are represented by these different proxies.

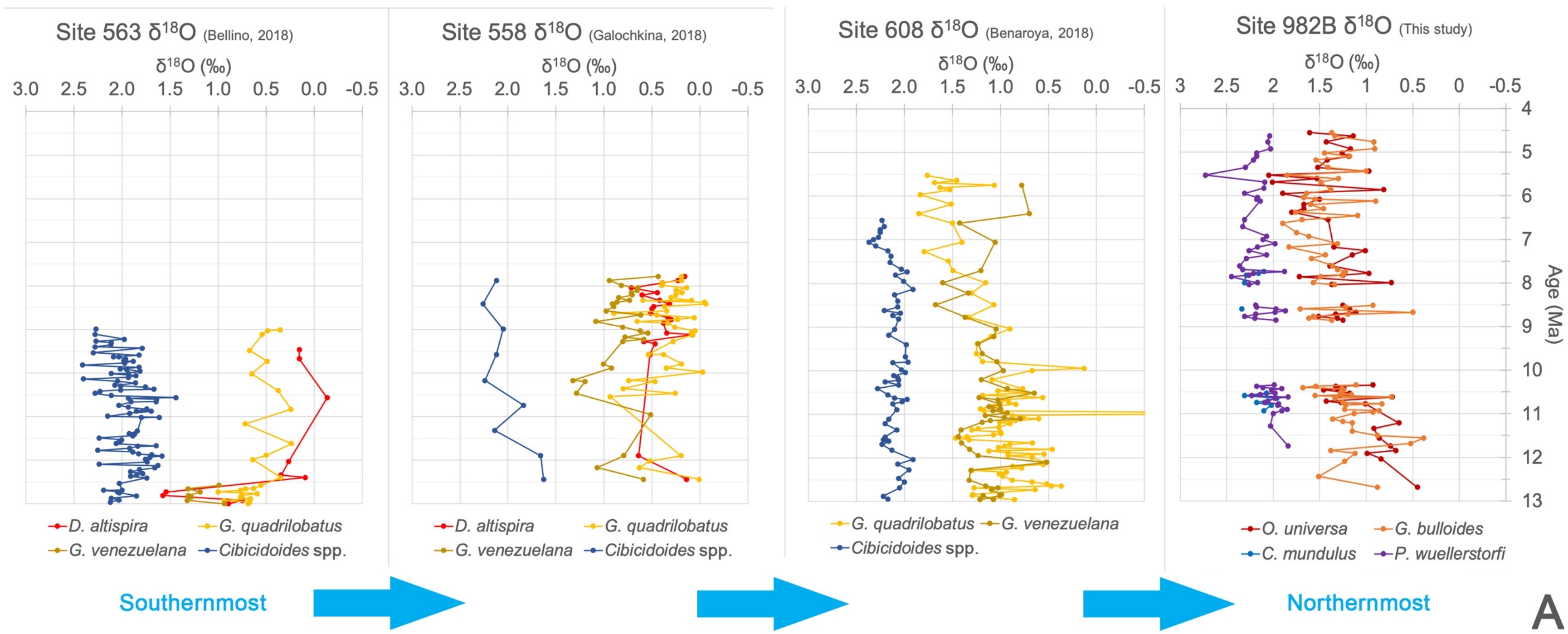
Site 563 δ18O (Bellino, 2018)
Site 558 δ18O (Galochkina, 2018)
Site 608 δ18O (Benaroya, 2018)
Site 982B δ18O (This study)
δ18O (‰)
Age (Ma)
D. altispira
G. quadrilobatus
G. venezuelana
Cibicidoides spp.
O. universa
G. bulloides
C. mundulus
P. wuellerstorfi
Southernmost
Northernmost
A

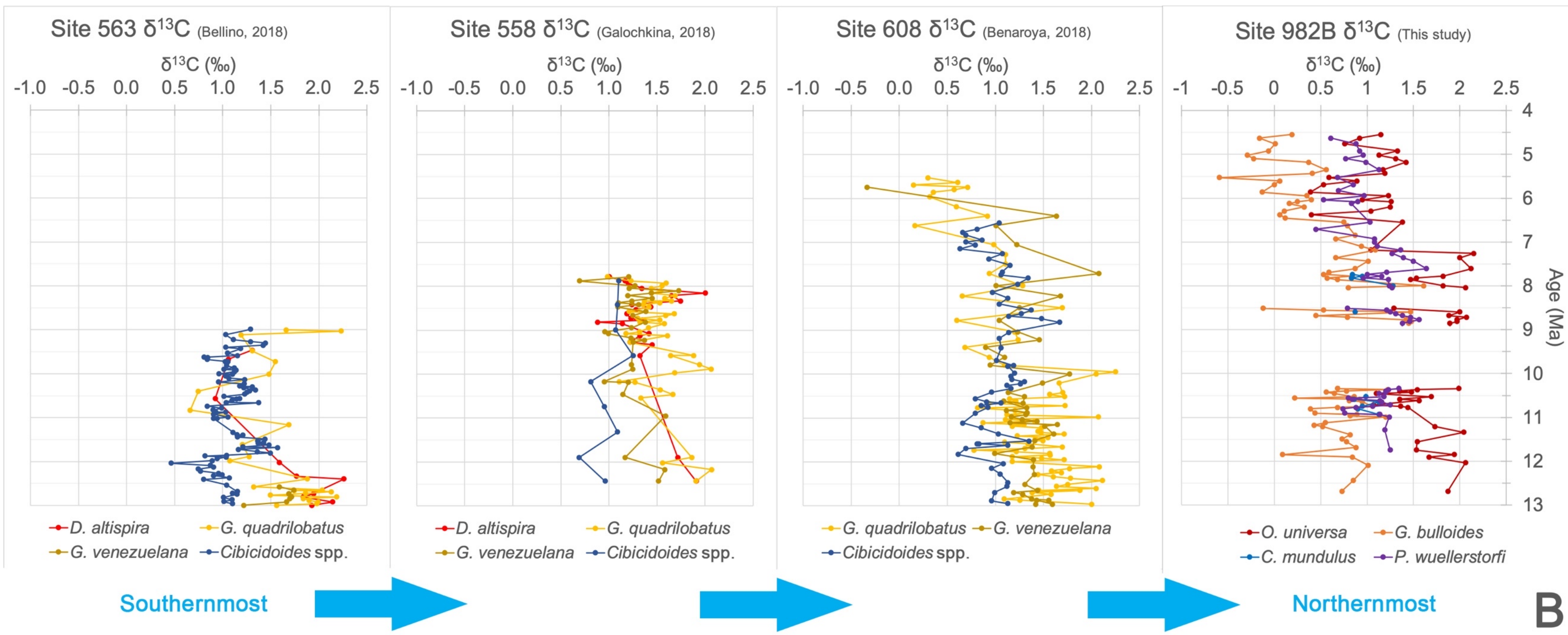

Figure 14. Comparison of stable isotope data from all sites in the WNAT. Only data within the time range covered by this study are shown. **A)** $\delta^{18}O$ values across the WNAT. **B)** $\delta^{13}C$ values across the WNAT. (Adapted from Bellino et al., 2018; Benaroya et al., 2018; Galochkina et al., 2017; 2018)

APPENDIX

Core	Section	Interval (cm)		Depth (mbsf)	Age (Ma)	Foraminifera			
		Top	Bottom			*O. universa*	*Gg. bulloides*	*C. mundulus*	*P. wuellerstorfi*
15	2	70	72	131.2	4.546	**8**	**10**	6	-
15	3	71	74	132.71	4.587	10	10	10	-
15	4	69	71	134.19	4.626	**9**	**10**	10	**5**
15	5	68	70	135.68	4.666	10	3	10	3
16	1	69	71	139.19	4.761	**10**	**10**	10	**10**
16	2	70	72	140.7	4.801	10	10	10	-
16	5	70	72	145.2	4.922	**8**	**5**	4	**4**
16	6	70	72	146.7	4.962	10	10	7	10
17	1	70	72	148.7	5.016	**10**	**10**	10	**8**
17	2	70	72	150.2	5.056	10	10	10	10
17	3	67	69	151.67	5.096	**4**	**9**	5	**10**
17	4	68	70	153.18	5.136	10	10	10	-
17	5	70	72	154.7	5.177	**10**	**10**	10	**6**
18	1	70	72	158.2	5.271	10	4	6	10
18	2	68	71	159.68	5.311	10	10	6	3
18	3	72	75	161.22	5.352	**9**	**10**	10	**5**
18	4	70	72	162.7	5.392	10	10	10	9
18	5	70	72	164.2	5.433	**9**	**9**	7	-
18	6	74	76	165.74	5.474	10	4	10	-
19	1	72	74	167.72	5.527	**7**	**6**	3	**3**
19	2	70	72	169.2	5.567	10	10	10	-
19	3	70	72	170.7	5.607	**10**	**10**	10	-
19	4	70	72	172.2	5.648	9	10	10	-
19	5	68	70	173.68	5.687	**3**	**10**	10	**7**
19	6	70	72	175.2	5.728	10	10	10	7
20	1	70	72	177.2	5.782	**SFT**	**SFT**	10	**8**
20	2	70	72	178.7	5.822	10	10	10	**3**
20	3	70	72	180.2	5.862	**4**	**10**	10	-
20	4	69	71	181.69	5.902	3	10	10	7
20	5	72	74	183.22	5.944	**3**	**7**	10	**10**
20	6	72	74	184.72	5.984	-	6	10	10
21	1	73	75	186.73	6.038	**3**	**9**	-	**7**
21	2	72	74	188.22	6.078	**9**	**3**	4	**10**

21	3	76	78	189.76	6.119	-	**8**	-	**10**
21	4	68	70	191.18	6.157				
21	5	73	75	192.73	6.199	**9**	**5**	10	-
21	6	73	75	194.23	6.239				
22	1	72	74	196.22	6.293	**10**	**7**	10	**10**
22	2	72	74	197.72	6.333				
22	3	83	85	199.33	6.376	**4**	**4**	4	-
22	4	71	73	200.71	6.413				
22	5	67	69	202.17	6.453	-	**7**	-	**6**
22	6	68	70	203.68	6.493				
23	1	73	75	205.73	6.548	**3**	**6**	-	**4**
23	2	73	75	207.23	6.589				
23	3	72	74	208.72	6.629	-	**7**	-	-
23	4	64	66	210.14	6.667				
23	5	73	75	211.73	6.710	-	-	-	**6**
24	1	65	67	215.15	6.801				
24	2	73	75	216.73	6.844	-	**5**	-	**8**
24	3	63	65	218.13	6.882				
24	4	73	75	219.73	6.925	-	**8**	5	**8**
24	5	73	75	221.23	6.965				
24	6	72	74	222.72	7.005	-	-	5	**10**
25	1	72	74	224.72	7.059				
25	2	72	74	226.22	7.099	-	**3**	9	**10**
25	3	72	74	227.72	7.139				
25	4	67	69	229.17	7.178	**5**	**3**	-	**7**
25	5	63	65	230.63	7.217				
25	6	67	69	232.17	7.259	**7**	-	3	**10**
26	1	73	75	234.23	7.314				
26	2	77	79	235.77	7.355	**6**	**4**	10	**8**
26	3	62	64	237.12	7.392				
26	4	73	75	238.73	7.435	**3**	**9**	10	**5**
26	5	67	69	240.17	7.474				
26	6	73	75	241.73	7.516	-	-	10	-
27	1	73	75	243.73	7.569				
27	2	71	73	245.21	7.609	**10**	**10**	10	**4**
27	3	81	83	246.81	7.652				
27	4	70	72	248.2	7.689	-	**7**	10	**6**
28	1	67	69	249.97	7.737	-	**7**	**5**	**5**
28	2	68	70	251.48	7.778	**5**	**7**	**8**	**9**

28	3	76	78	253.06	7.820	**3**	**6**	**8**	**6**
28	4	67	69	254.47	7.858	**3**	**4**	10	**3**
29	1	69	71	259.59	7.995	**3**	**7**	**5**	**3**
29	2	71	73	261.11	8.036	**8**	**7**	-	**6**
31	1	68	70	278.88	8.514	**3**	**6**	-	**10**
31	2	63	65	280.33	8.553	-	**7**	-	**10**
31	3	72	74	281.92	8.595	**6**	**9**	**5**	**9**
31	4	72	74	283.42	8.636	3	10	4	**10**
31	5	72	74	284.92	8.676	**8**	**10**	-	**9**
31	6	67	69	286.37	8.715	**7**	**9**	8	**10**
32	1	62	64	288.42	8.770	**10**	**6**	9	**10**
32	2	70	72	290	8.812	**10**	**10**	-	**8**
32	3	71	73	291.51	8.853	**10**	**8**	-	**10**
33	1	76	78	298.16	10.339	**9**	**10**	5	**7**
33	2	70	72	299.6	10.367	**9**	**5**	-	**11**
33	3	76	78	301.16	10.398	**9**	**3**	4	**10**
33	4	72	74	302.62	10.426	**3**	**8**	-	**8**
33	5	66	68	304.06	10.454	**4**	**5**	4	**10**
34	1	72	74	307.82	10.528	**10**	**7**	**8**	**10**
34	2	73	75	309.33	10.557	**9**	**7**	6	**7**
34	3	68	70	310.78	10.586	**10**	**9**	**5**	**10**
34	4	78	80	312.38	10.617	**10**	**4**	10	**4**
34	5	72	74	313.82	10.645	-	**10**	**5**	**10**
35	1	60	62	317.3	10.713	**4**	-	10	**5**
35	2	68	70	318.88	10.744	**10**	**7**	**3**	**9**
35	3	67	69	320.37	10.773	**9**	**4**	10	**10**
35	4	81	83	322.01	10.805	-	**10**	**5**	**10**
36	1	77	79	327.07	10.904	-	**6**	10	**10**
36	2	73	75	328.53	10.933	-	**10**	**3**	**10**
36	3	77	79	330.07	10.963	-	**7**	10	10
36	4	72	74	331.52	10.991	-	**8**	**10**	**10**
37	1	69	71	336.69	11.092	-	3	10	-
37	2	68	70	338.18	11.121	-	**8**	10	10
37	3	77	79	339.77	11.153	3	7	9	10
37	4	67	69	341.17	11.180	**9**	**6**	10	10
37	5	66	68	342.66	11.209	**7**	**3**	5	7
38	1	69	71	346.29	11.280	-	-	10	**10**
38	2	69	71	347.79	11.309				
38	3	63	65	349.23	11.338	**9**	**3**	10	7

38	4	68	70	350.78	11.368	-	**3**	8	-
38	5	72	74	352.32	11.398	-	**3**	8	10
39	1	63	65	355.83	11.467	-	-	9	8
39	2	66	68	357.36	11.496	-	**8**	7	6
39	3	64	66	358.84	11.525	-	3	6	9
39	4	62	64	360.32	11.554	**3**	**8**	10	10
40	1	67	69	365.57	11.657	-	-	-	4
40	2	67	69	367.07	11.686	-	**4**	10	10
40	3	68	70	368.58	11.716	-	-	10	10
40	4	67	69	370.07	11.745	**7**	-	9	**9**
41	1	70	72	375.2	11.845				
41	1	73	75	375.23	11.846	**9**	**3**	10	10
41	2	67	69	376.67	11.874	-	-	5	5
41	3	73	75	378.23	11.905	**3**	**7**	10	10
41	4	68	70	379.68	11.933	-	3	8	10
42	1	73	75	384.83	12.034	**5**	-	10	10
42	2	77	79	386.37	12.064	3	-	9	9
42	3	77	79	387.87	12.093	-	**4**	10	10
42	4	76	78	389.36	12.122	-	-	5	-
43	1	66	68	394.46	12.222	-	-	4	6
43	3	77	79	397.57	12.283	-	5	4	7
44	2	71	73	405.61	12.440	-	**7**	-	6
44	4	68	70	408.58	12.498	-	5	10	9
45	4	70	72	418.2	12.686	**4**	**8**	-	**10**

Table 1. Numbers in the "Foraminifera" columns represent the number of individuals of each species that were picked from each sample. Green cells indicate that the isotope data was obtained from these picked individuals. Red cells represent picked individuals that were lost due to issues with the mass spectrometer. Cells filled with a dash (-) indicated that only 0-2 individuals of the given species were found in the given sample. Note that not all 134 samples obtained from the Bremen Core Repository were fully processed; samples that were not fully processed are represented by blank cells in the "Foraminifera" columns in this table and were excluded from other tables in this APPENDIX.

Core	Section	Interval (cm)		Depth (mbsf)	Age (Ma)	Original Weight (g)	Washed Weight (g)	Coarse Fraction
		Top	Bottom					
15	2	70	72	131.2	4.546	30.8	1.0	3.25%
15	3	71	74	132.71	4.587	31.5	1.1	3.49%
15	4	69	71	134.19	4.626	31.0	1.1	3.55%
15	5	68	70	135.68	4.666	30.8	0.8	2.60%
16	1	69	71	139.19	4.761	29.3	0.9	3.07%
16	2	70	72	140.7	4.801	21.7	1.8	8.29%
16	5	70	72	145.2	4.922	11.6	0.4	3.45%
16	6	70	72	146.7	4.962	21.2	1.0	4.72%
17	1	70	72	148.7	5.016	24.9	1.1	4.42%
17	2	70	72	150.2	5.056	25.2	0.7	2.78%
17	3	67	69	151.67	5.096	34.2	1.0	2.92%
17	4	68	70	153.18	5.136	23.8	1.1	4.62%
17	5	70	72	154.7	5.177	33.4	1.5	4.49%
18	1	70	72	158.2	5.271	26.8	0.7	2.61%
18	2	68	71	159.68	5.311	10.2	0.3	2.94%
18	3	72	75	161.22	5.352	18.8	0.7	3.72%
18	4	70	72	162.7	5.392	29.3	1.5	5.12%
18	5	70	72	164.2	5.433	22.4	0.9	4.02%
18	6	74	76	165.74	5.474	21.8	0.6	2.75%
19	1	72	74	167.72	5.527	7.5	0.5	6.67%
19	2	70	72	169.2	5.567	22.4	2.2	9.82%
19	3	70	72	170.7	5.607	19.1	2.0	10.47%
19	4	70	72	172.2	5.648	19.3	1.8	9.33%
19	5	68	70	173.68	5.687	28.5	1.3	4.56%

19	6	70	72	175.2	5.728	48.3	1.4	2.90%
20	1	70	72	177.2	5.782	31.1	3.7	11.90%
20	2	70	72	178.7	5.822	39.9	2.5	6.27%
20	3	70	72	180.2	5.862	27.6	0.9	3.26%
20	4	69	71	181.69	5.902	27.4	1.1	4.01%
20	5	72	74	183.22	5.944	36.8	0.5	1.36%
20	6	72	74	184.72	5.984	38.8	1.4	3.61%
21	1	73	75	186.73	6.038	27.0	0.4	1.48%
21	2	72	74	188.22	6.078	22.5	1.0	4.44%
21	3	76	78	189.76	6.119	31.0	1.0	3.23%
21	4	68	70	191.18	6.157	33.3	1.4	4.20%
21	5	73	75	192.73	6.199	26.4	0.9	3.41%
21	6	73	75	194.23	6.239	28.4	0.9	3.17%
22	1	72	74	196.22	6.293	37.6	1.6	4.26%
22	2	72	74	197.72	6.333	21.3	1.0	4.69%
22	3	83	85	199.33	6.376	23.6	0.7	2.97%
22	4	71	73	200.71	6.413	22.8	0.4	1.75%
22	5	67	69	202.17	6.453	26.0	0.8	3.08%
22	6	68	70	203.68	6.493	22.6	0.6	2.65%
23	1	73	75	205.73	6.548	34.8	1.3	3.74%
23	2	73	75	207.23	6.589	34.9	1.7	4.87%
23	3	72	74	208.72	6.629	44.7	1.3	2.91%
23	4	64	66	210.14	6.667	31.0	1.4	4.52%
23	5	73	75	211.73	6.710	22.1	1.1	4.98%
24	1	65	67	215.15	6.801	34.2	1.9	5.56%
24	2	73	75	216.73	6.844	39.4	1.7	4.31%
24	3	63	65	218.13	6.882	33.1	1.3	3.93%

24	4	73	75	219.73	6.925	29.4	1.7	5.78%
24	5	73	75	221.23	6.965	46.3	1.9	4.10%
24	6	72	74	222.72	7.005	15.9	0.5	3.14%
25	1	72	74	224.72	7.059	28.5	0.5	1.75%
25	2	72	74	226.22	7.099	45.7	1.1	2.41%
25	3	72	74	227.72	7.139	29.7	0.9	3.03%
25	4	67	69	229.17	7.178	4.8	0.1	2.08%
25	5	63	65	230.63	7.217	34.4	1.0	2.91%
25	6	67	69	232.17	7.259	35.3	0.7	1.98%
26	1	73	75	234.23	7.314	33.3	0.8	2.40%
26	2	77	79	235.77	7.355	36.0	1.1	3.06%
26	3	62	64	237.12	7.392	38.3	1.2	3.13%
26	4	73	75	238.73	7.435	28.4	1.1	3.87%
26	5	67	69	240.17	7.474	24.2	1.2	4.96%
26	6	73	75	241.73	7.516	26.4	0.9	3.41%
27	1	73	75	243.73	7.569	24.3	0.6	2.47%
27	2	71	73	245.21	7.609	24.4	1.0	4.10%
27	3	81	83	246.81	7.652	28.1	0.9	3.20%
27	4	70	72	248.2	7.689	9.1	0.4	4.40%
28	1	67	69	249.97	7.737	30.1	1.0	3.32%
28	2	68	70	251.48	7.778	28.0	1.1	3.93%
28	3	76	78	253.06	7.820	36.9	1.2	3.25%
28	4	67	69	254.47	7.858	38.7	1.3	3.36%
29	1	69	71	259.59	7.995	19.5	1.2	6.15%
29	2	71	73	261.11	8.036	12.3	1.0	8.13%
31	1	68	70	278.88	8.514	17.1	0.5	2.92%
31	2	63	65	280.33	8.553	28.8	1.1	3.82%

31	3	72	74	281.92	8.595	27.9	0.7	2.51%
31	4	72	74	283.42	8.636	10.7	0.5	4.67%
31	5	72	74	284.92	8.676	30.4	0.7	2.30%
31	6	67	69	286.37	8.715	38.4	1.6	4.17%
32	1	62	64	288.42	8.770	21.4	1.2	5.61%
32	2	70	72	290	8.812	17.7	1.1	6.21%
32	3	71	73	291.51	8.853	32.2	1.7	5.28%
33	1	76	78	298.16	10.339	27.0	2.7	10.00%
33	2	70	72	299.6	10.367	27.4	3.1	11.31%
33	3	76	78	301.16	10.398	22.8	1.9	8.33%
33	4	72	74	302.62	10.426	7.8	0.6	7.69%
33	5	66	68	304.06	10.454	14.2	1.0	7.04%
34	1	72	74	307.82	10.528	24.3	2.4	9.88%
34	2	73	75	309.33	10.557	32.6	2.4	7.36%
34	3	68	70	310.78	10.586	15.1	1.9	12.58%
34	4	78	80	312.38	10.617	30.7	2.5	8.14%
34	5	72	74	313.82	10.645	33.3	2.3	6.91%
35	1	60	62	317.3	10.713	7.1	0.5	7.04%
35	2	68	70	318.88	10.744	28.6	1.6	5.59%
35	3	67	69	320.37	10.773	28.8	2.2	7.64%
35	4	81	83	322.01	10.805	21.2	2.5	11.79%
36	1	77	79	327.07	10.904	43.6	1.4	3.21%
36	2	73	75	328.53	10.933	17.6	0.8	4.55%
36	3	77	79	330.07	10.963	17.7	0.8	4.52%
36	4	72	74	331.52	10.991	22.6	1.3	5.75%
37	1	69	71	336.69	11.092	8.1	1.0	12.35%
37	2	68	70	338.18	11.121	46.5	3.2	6.88%

37	3	77	79	339.77	11.153	30.2	1.9	6.29%
37	4	67	69	341.17	11.180	37.0	2.2	5.95%
37	5	66	68	342.66	11.209	43.0	2.0	4.65%
38	1	69	71	346.29	11.280	15.3	0.9	5.88%
38	2	69	71	347.79	11.309	39.3	2.1	5.34%
38	3	63	65	349.23	11.338	31.2	2.0	6.41%
38	4	68	70	350.78	11.368	35.6	1.3	3.65%
38	5	72	74	352.32	11.398	32.1	1.6	4.98%
39	1	63	65	355.83	11.467	28.2	2.3	8.16%
39	2	66	68	357.36	11.496	16.5	1.8	10.91%
39	3	64	66	358.84	11.525	19.4	3.0	15.46%
39	4	62	64	360.32	11.554	26.2	2.6	9.92%
40	1	67	69	365.57	11.657	8.5	0.5	5.88%
40	2	67	69	367.07	11.686	29.7	3.1	10.44%
40	3	68	70	368.58	11.716	17.3	2.1	12.14%
40	4	67	69	370.07	11.745	31.1	2.0	6.43%
41	1	70	72	375.2	11.845	38.1	2.4	6.30%
41	1	73	75	375.23	11.846	21.8	2.6	11.93%
41	2	67	69	376.67	11.874	21.2	2.4	11.32%
41	3	73	75	378.23	11.905	25.3	2.0	7.91%
41	4	68	70	379.68	11.933	12.8	0.7	5.47%
42	1	73	75	384.83	12.034	18.0	0.5	2.78%
42	2	77	79	386.37	12.064	13.4	0.7	5.22%
42	3	77	79	387.87	12.093	25.3	1.3	5.14%
42	4	76	78	389.36	12.122	8.3	0.2	2.41%
43	1	66	68	394.46	12.222	11.1	0.3	2.70%
43	3	77	79	397.57	12.283	15.2	0.7	4.61%

44	2	71	73	405.61	12.440	8.9	0.3	3.37%
44	4	68	70	408.58	12.498	8.5	0.7	8.24%
45	4	70	72	418.2	12.686	10.9	0.6	5.50%

Table 2. Coarse (>63 μm) fraction data from all 134 samples. Percent values are fractions of the original mass of each sample. These data are plotted in **Fig. 4**.

Interval	Sedimentation Rate (m/Ma)	Equation	Depth Range (mbsf)	Age Range (Ma)
1	21.96	y = 21.96x	0 - 54.68	0 - 2.49
2	37.22	y = 37.22x - 2033	54.68 - 293.62	2.49 - 8.91
3	51.14	y = 51.14x - 15007	293.62 - 450.12	10.25 - 13.31
4	25.15	y = 25.15x - 11306	450.12 - 566.80	13.31 - 17.95

Table 3. Sedimentation equations for each interval in the age model (**Fig. 7**) used in this study. Note the hiatus between Intervals 3 and 4. (Jansen et al., 1996; ODSN, 2011; Gradstein et al., 2012)

Core	Section	Interval (cm)		Depth (mbsf)	Age (Ma)	$\delta^{13}C$ PDB (‰)				$\delta^{18}O$ PDB (‰)			
		Top	Bottom			*O. universa*	*Gg. bulloides*	*C. mundulus*	*P. wuellerstorfi*	*O. universa*	*Gg. bulloides*	*C. mundulus*	*P. wuellerstorfi*
15	2	70	72	131.2	4.546	1.15	0.19			1.61	1.37		
15	4	69	71	134.19	4.626	0.92	-0.16		0.61	1.14	1.34		2.04
16	1	69	71	139.19	4.761	0.76	0.01		0.88	1.43	0.92		2.06
16	5	70	72	145.2	4.922	1.33	-0.06		0.92	1.17	0.91		2.03
17	1	70	72	148.7	5.016	1.13	-0.29		0.96	1.26	1.45		2.18
17	3	67	69	151.67	5.096	1.31	-0.22		0.77	1.19	1.18		2.18
17	5	70	72	154.7	5.177	1.42	0.37		0.99	1.42	1.54		2.21
18	3	72	75	161.22	5.352	1.17	0.56		1.13	1.52	1.41		2.3
18	5	70	72	164.2	5.433	1.19	0.41			0.97	1		
19	1	72	74	167.72	5.527	0.59	-0.59		0.68	2.05	1.85		2.73
19	3	70	72	170.7	5.607	0.89	0.06			1.53	1.3		
19	5	68	70	173.68	5.687	0.53	0		0.85	2.01	1.49		2.09
20	2	70	72	178.7	5.822				0.69				2.1
20	3	70	72	180.2	5.862	0.39	-0.13			0.81	1.38		
20	5	72	74	183.22	5.944	1.23	0.35		0.97	1.9	1.64		2.31
21	1	73	75	186.73	6.038	0.95	0.4		0.53	1.67	1.67		2.17
21	2	72	74	188.22	6.078	1.26	0.25		0.9	1.5	1.55		2.18
21	3	76	78	189.76	6.119		0.16		0.83		0.9		2.14
21	5	73	75	192.73	6.199	1.25	0.32			1.67	1.6		
22	1	72	74	196.22	6.293	1.04	0.11			1.67	1.46		
22	3	83	85	199.33	6.376	0.4	0.06			1.8	1.76		
22	5	67	69	202.17	6.453		0.12				1.09		
23	1	73	75	205.73	6.548	1.38	0.75		1.03	1.41	1.69		2.31

23	3	72	74	208.72	6.629		0.79				1.9		
23	5	73	75	211.73	6.710				0.45				2.33
24	2	73	75	216.73	6.844		0.87				1.75		
24	4	73	75	219.73	6.925		0.66		1.08		1.62		2.07
24	6	72	74	222.72	7.005				1.08				2.11
25	2	72	74	226.22	7.099		0.94		1.11		1.31		1.98
25	4	67	69	229.17	7.178	1.04	1.09		1.36	1.35	1.83		2.17
25	6	67	69	232.17	7.259	2.15			1.27	1.01			2.26
26	2	77	79	235.77	7.355	2	0.66		1.39	1.15	1.44		2.07
26	4	73	75	238.73	7.435		1.01		1.5		1.59		2.29
27	2	71	73	245.21	7.609	2.12	0.87		1.64	1.39	1.36		2.36
27	4	70	72	248.2	7.689		0.59		1.21		1.31		2.33
28	1	67	69	249.97	7.737		0.53	0.84	1		1.22	2.1	1.88
28	2	68	70	251.48	7.778	1.82	0.84	0.95	1.16	0.97	1.24	2.16	2.21
28	3	76	78	253.06	7.820	1.53	0.57	0.83	0.96	1.25	1.26	2.29	2.26
28	4	67	69	254.47	7.858	1.47	0.68		1.23	1.72	1.49		2.45
29	1	69	71	259.59	7.995	1.82	1.61	1.28	1.24	0.73	1.57	2.31	2.17
29	2	71	73	261.11	8.036	2.06	0.8		1.27	1.37	1.34		2.26
31	1	68	70	278.88	8.514	1.29	-0.12		0.79	1.25	0.93		2.19
31	2	63	65	280.33	8.553		0.53		1.21		1.22		2.18
31	3	72	74	281.92	8.595	2	1.47	0.87	1.25	1.18	1.71	2.34	1.97
31	4	72	74	283.42	8.636				1.31				1.87
31	5	72	74	284.92	8.676	1.88	0.45		1.38	1.11	0.5		1.98
31	6	67	69	286.37	8.715	2.07	0.79		1.47	1.33	1.2		2.19
32	1	62	64	288.42	8.770	1.97	1.42		1.56	1.51	1.57		2.31
32	2	70	72	290	8.812	1.97	1.48		1.46	1.31	1.62		2.2
32	3	71	73	291.51	8.853	1.89	1.45		1.38	1.25	1.37		1.97

33	1	76	78	298.16	10.339	1.99	0.68		1.34	0.93	1.11		1.99
33	2	70	72	299.6	10.367	1.54	1.22		1.23	1.33	1.54		2.18
33	3	76	78	301.16	10.398	1.35	0.78		1.2	1.24	1.68		2.11
33	4	72	74	302.62	10.426	1.48	0.56		1.2	1.31	1.26		1.91
33	5	66	68	304.06	10.454	1.1	0.65		1.13	1.46	1.24		2.02
34	1	72	74	307.82	10.528	1.69	0.86	0.99	1.18	1.18	1.28	2.07	1.98
34	2	73	75	309.33	10.557		0.22		0.8		1.16		2.14
34	3	68	70	310.78	10.586	1.35	0.92	0.86	0.84	1.28	1.55	2.31	2.23
34	4	78	80	312.38	10.617	1.56	0.81		1.14	0.72	0.73		1.84
34	5	72	74	313.82	10.645		0.95	1.13	1.16		1.34	1.96	1.98
35	1	60	62	317.3	10.713	1.07			1.25	1.43			2.06
35	2	68	70	318.88	10.744	1.36	1.06	0.95	1.06	1.27	1.25	2.18	2.09
35	3	67	69	320.37	10.773	1.44	0.68		0.88	1.01	0.83		1.94
35	4	81	83	322.01	10.805		0.39	0.9	0.74		1.22	2.02	1.95
36	1	77	79	327.07	10.904		0.44		0.76		1.23		1.85
36	2	73	75	328.53	10.933		0.89	1.13	1.14		0.86	2.1	1.91
36	3	77	79	330.07	10.963		0.82				0.93		
36	4	72	74	331.52	10.991		1.2		1.24		1.13		2
37	2	68	70	338.18	11.121		0.55				1.36		
37	4	67	69	341.17	11.180		0.43				1.25		
37	5	66	68	342.66	11.209	1.73	0.52			0.65	1.15		
38	1	69	71	346.29	11.280				1.19				2.03
38	3	63	65	349.23	11.338	2.04				0.92			
38	5	72	74	352.32	11.398		0.82				1.15		
39	2	66	68	357.36	11.496		0.73				0.88		
39	4	62	64	360.32	11.554	1.54	0.78			0.86	0.38		
40	2	67	69	367.07	11.686		0.88				0.52		

40	4	67	69	370.07	11.745	1.53			1.25	0.74			1.84
41	1	73	75	375.23	11.846	1.94	0.09			0.68	1.38		
41	3	73	75	378.23	11.905	1.67	0.84			0.99	1.12		
42	1	73	75	384.83	12.034	2.06				0.84			
42	3	77	79	387.87	12.093		1.01				1.23		
44	2	71	73	405.61	12.440		0.85				1.51		
45	4	70	72	418.2	12.686	1.87	0.73			0.45	0.88		

Table 4. Isotope data from each fully processed sample. These data are plotted in **Figs. 8** and **9**.

Core	Section	Interval (cm)		Depth (mbsf)	Age (Ma)	$\delta^{18}O$ PDB (per mil)				$\delta^{18}O_{seawater}$ (Cramer et al., 2011)	Temperatures (°C)			
		Top	Bottom			*O. universa*	*Gg. bulloides*	*C. mundulus*	*P. wuellerstorfi*		*O. universa*	*Gg. bulloides*	*C. mundulus*	*P. wuellerstorfi*
15	2	70	72	131.2	4.546	1.61	1.37			-0.0038	8.85	9.90		
15	4	69	71	134.19	4.626	1.14	1.34		2.04	0.0403	11.11	10.22		7.18
16	1	69	71	139.19	4.761	1.43	0.92		2.06	0.1061	10.11	12.38		7.38
16	5	70	72	145.2	4.922	1.17	0.91		2.03	0.1174	11.32	12.48		7.55
17	1	70	72	148.7	5.016	1.26	1.45		2.18	0.0704	10.71	9.87		6.71
17	3	67	69	151.67	5.096	1.19	1.18		2.18	0.0431	10.90	10.94		6.60
17	5	70	72	154.7	5.177	1.42	1.54		2.21	0.0426	9.88	9.35		6.47
18	3	72	75	161.22	5.352	1.52	1.41		2.3	0.1045	9.71	10.20		6.35
18	5	70	72	164.2	5.433	0.97	1			0.1162	12.20	12.07		
19	1	72	74	167.72	5.527	2.05	1.85		2.73	0.1117	7.44	8.31		4.57
19	3	70	72	170.7	5.607	1.53	1.3			0.0950	9.63			
19	5	68	70	173.68	5.687	2.01	1.49		2.09	0.0669	7.42	9.68		7.08
20	2	70	72	178.7	5.822				2.1	0.0521				6.98
20	3	70	72	180.2	5.862	0.81	1.38			0.0572	12.66	10.12		
20	5	72	74	183.22	5.944	1.9	1.64		2.31	0.0788	7.95	9.08		6.20
21	1	73	75	186.73	6.038	1.67	1.67		2.17	0.1102	9.08	9.08		6.92
21	2	72	74	188.22	6.078	1.5	1.55		2.18	0.1218	9.88	9.66		6.93
21	3	76	78	189.76	6.119		0.9		2.14	0.1317		12.59		7.14
21	5	73	75	192.73	6.199	1.67	1.6			0.1424	9.22	9.53		
22	1	72	74	196.22	6.293	1.67	1.46			0.1466	9.24	10.16		
22	3	83	85	199.33	6.376	1.8	1.76			0.1560	8.72	8.89		
22	5	67	69	202.17	6.453		1.09			0.1657		11.89		
23	1	73	75	205.73	6.548	1.41	1.69		2.31	0.1610	10.44	9.22		6.54

23	3	72	74	208.72	6.629		1.9			0.1412		8.22		
23	5	73	75	211.73	6.710				2.33	0.1253				6.31
24	2	73	75	216.73	6.844		1.75			0.1212		8.78		
24	4	73	75	219.73	6.925		1.62		2.07	0.1115		9.31		7.36
24	6	72	74	222.72	7.005				2.11	0.1063				7.16
25	2	72	74	226.22	7.099		1.31		1.98	0.1140		10.68		7.75
25	4	67	69	229.17	7.178	1.35	1.83		2.17	0.1057	10.47	8.37		6.90
25	6	67	69	232.17	7.259	1.01			2.26	0.0743	11.84			6.39
26	2	77	79	235.77	7.355	1.15	1.44		2.07	0.0377	11.05	9.77		7.04
26	4	73	75	238.73	7.435		1.59		2.29	0.0464		9.15		6.14
27	2	71	73	245.21	7.609	1.39	1.36		2.36	0.1561	10.51	10.64		6.31
27	4	70	72	248.2	7.689		1.31		2.33	0.2058		11.09		6.65
28	1	67	69	249.97	7.737		1.22	2.1	1.88	0.2312		11.60	7.74	8.69
28	2	68	70	251.48	7.778	0.97	1.24	2.16	2.21	0.2473	12.79	11.58	7.55	7.34
28	3	76	78	253.06	7.820	1.25	1.26	2.29	2.26	0.2657	11.62	11.58	7.08	7.20
28	4	67	69	254.47	7.858	1.72	1.49		2.45	0.2857	9.63	10.64		6.48
29	1	69	71	259.59	7.995	0.73	1.57	2.31	2.17	0.3075	14.16	10.39	7.17	7.77
29	2	71	73	261.11	8.036	1.37	1.34		2.26	0.2973	11.23	11.36		7.34
31	1	68	70	278.88	8.514	1.25	0.93		2.19	0.3614	12.05	13.49		7.92
31	2	63	65	280.33	8.553		1.22		2.18	0.3622		12.19		7.96
31	3	72	74	281.92	8.595	1.18	1.71	2.34	1.97	0.3645	12.38	10.02	7.28	8.88
31	4	72	74	283.42	8.636				1.87	0.3641				9.32
31	5	72	74	284.92	8.676	1.11	0.5		1.98	0.3601	12.67	15.45		8.82
31	6	67	69	286.37	8.715	1.33	1.2		2.19	0.3554	11.66	12.25		7.89
32	1	62	64	288.42	8.770	1.51	1.57		2.31	0.3544	10.86	10.59		7.37
32	2	70	72	290	8.812	1.31	1.62		2.2	0.3629	11.79	10.41		7.88
32	3	71	73	291.51	8.853	1.25	1.37		1.97	0.3697	12.09	11.55		8.91

33	1	76	78	298.16	10.339	0.93	1.11		1.99	0.0511	12.09	11.29		7.44
33	2	70	72	299.6	10.367	1.33	1.54		2.18	0.0463	10.29	9.37		6.61
33	3	76	78	301.16	10.398	1.24	1.68		2.11	0.0353	10.64	8.71		6.86
33	4	72	74	302.62	10.426	1.31	1.26		1.91	0.0293	10.30	10.53		7.69
33	5	66	68	304.06	10.454	1.46	1.24		2.02	0.0174	9.59	10.56		7.17
34	1	72	74	307.82	10.528	1.18	1.28	2.07	1.98	0.0010	10.75	10.31	6.89	7.27
34	2	73	75	309.33	10.557		1.16		2.14	-0.0111		10.79		6.54
34	3	68	70	310.78	10.586	1.28	1.55	2.31	2.23	-0.0186	10.23	9.04	5.78	6.12
34	4	78	80	312.38	10.617	0.72	0.73		1.84	-0.0380	12.63	12.59		7.70
34	5	72	74	313.82	10.645		1.34	1.96	1.98	-0.0498		9.83	7.14	7.05
35	1	60	62	317.3	10.713	1.43			2.06	-0.0958	9.23			6.52
35	2	68	70	318.88	10.744	1.27	1.25	2.18	2.09	-0.1027	9.90	9.99	5.98	6.36
35	3	67	69	320.37	10.773	1.01	0.83		1.94	-0.1069	11.03	11.83		6.98
35	4	81	83	322.01	10.805		1.22	2.02	1.95	-0.1044		10.11	6.65	6.95
36	1	77	79	327.07	10.904		1.23		1.85	-0.0696		10.22		7.52
36	2	73	75	328.53	10.933		0.86	2.1	1.91	-0.0548		11.93	6.52	7.33
36	3	77	79	330.07	10.963		0.93			-0.0477		11.65		
36	4	72	74	331.52	10.991		1.13		2	-0.0341		10.82		7.03
37	2	68	70	338.18	11.121		1.36			-0.0091		9.92		
37	4	67	69	341.17	11.180		1.25			-0.0144		10.38		
37	5	66	68	342.66	11.209	0.65	1.15			-0.0177	13.04	10.80		
38	1	69	71	346.29	11.280				2.03	-0.0243				6.95
38	3	63	65	349.23	11.338	0.92				-0.0183	11.83			
38	5	72	74	352.32	11.398		1.15			-0.0121		10.83		
39	2	66	68	357.36	11.496		0.88			-0.0152		12.02		
39	4	62	64	360.32	11.554	0.86	0.38			-0.0134	12.12	14.29		
40	2	67	69	367.07	11.686		0.52			0.0066		13.74		

40	4	67	69	370.07	11.745	0.74			1.84	0.0176	12.79			7.94
41	1	73	75	375.23	11.846	0.68	1.38			0.0373	13.15	10.03		
41	3	73	75	378.23	11.905	0.99	1.12			0.0336	11.74	11.17		
42	1	73	75	384.83	12.034	0.84				-0.0520	12.03			
42	3	77	79	387.87	12.093		1.23			-0.0895		10.13		
44	2	71	73	405.61	12.440		1.51			0.0151		9.36		
45	4	70	72	418.2	12.686	0.45	0.88			0.0434	14.23	12.28		

Table 5. Temperature values calculated from $\delta^{18}O$ values using the methodology outlined in **Stable isotope analyses** (Kim and O'Neil, 1997; Cramer et al., 2011). These data are plotted in **Fig**. **10**.